

Did the Paleo-Asian Ocean between North China Block and Mongolia Block exist during the Late Paleozoic? First paleomagnetic evidence from central-eastern Inner Mongolia, China

Pan Zhao, Yan Chen, Bei Xu, Michel Faure, Guanzhong Shi, Flavien Choulet

▶ **To cite this version:**

Pan Zhao, Yan Chen, Bei Xu, Michel Faure, Guanzhong Shi, et al.. Did the Paleo-Asian Ocean between North China Block and Mongolia Block exist during the Late Paleozoic? First paleomagnetic evidence from central-eastern Inner Mongolia, China. Journal of Geophysical Research : Solid Earth, 2013, 118, pp.1873-1894. 10.1002/jgrb.50198 . insu-00819742

HAL Id: insu-00819742

https://insu.hal.science/insu-00819742

Submitted on 20 Feb 2014

HAL is a multi-disciplinary open access archive for the deposit and dissemination of scientific research documents, whether they are published or not. The documents may come from teaching and research institutions in France or abroad, or from public or private research centers.

L'archive ouverte pluridisciplinaire **HAL**, est destinée au dépôt et à la diffusion de documents scientifiques de niveau recherche, publiés ou non, émanant des établissements d'enseignement et de recherche français ou étrangers, des laboratoires publics ou privés.

JOURNAL OF GEOPHYSICAL RESEARCH: SOLID EARTH, VOL. 118, 1873–1894, doi:10.1002/jgrb.50198, 2013

Did the Paleo-Asian Ocean between North China Block and Mongolia Block exist during the late Paleozoic? First paleomagnetic evidence from central-eastern Inner Mongolia, China

Pan Zhao,[1,2] Yan Chen,[2] Bei Xu,[1] Michel Faure,[2] Guanzhong Shi,[1,2] and Flavien Choulet[2]

Received 13 December 2012; revised 18 April 2013; accepted 19 April 2013; published 30 May 2013.

[1] The tectonic evolution of the Paleo-Asian Ocean between the North China Block (NCB) and the Mongolia Block (MOB) is a contentious issue, and geodynamic models remain speculative. In an effort to puzzle out this controversy, a paleomagnetic study was carried out on the Silurian to Permian formations in central-eastern Inner Mongolia (China). More than 680 sedimentary and volcanic samples were collected from 86 sites. We have established titanium-poor magnetite and hematite as the principal magnetic carriers. Anisotropy of the magnetic susceptibility measurements demonstrate negligible deformation of the majority of study rocks with sedimentary fabrics. From primary magnetizations, a Late Devonian and a Permian pole are calculated for Inner Mongolia Block (IMB) at $\lambda = 46.8°$N, $\varphi = 349.1°$E, $dp = 14.6°$, $dm = 27.3°$ with $N = 3$ and $\lambda = 48.7°$N, $\varphi = 3.7°$E, $dp = 5.2°$, $dm = 9.1°$ with $N = 6$, respectively. Two stages of secondary magnetization are also identified probably due to Early Permian and Early Cretaceous magmatic events. As preliminary results, the comparison of our new paleomagnetic poles with available data from NCB, MOB, and Siberia indicates that (1) the paleolatitudes of IMB, NCB, and MOB are consistent between Late Devonian and Permian, suggesting pre-Late Devonian closure of the Paleo-Asian Ocean and further evaluation of these three blocks as a single entity and (2) post-Permian intracontinental deformation was significant and characterized by block rotations, which are due to strike-slip faulting within the welded NCB-IMB-MOB block.

Citation: Zhao, P., Y. Chen, B. Xu, M. Faure, G. Shi, and F. Choulet (2013), Did the Paleo-Asian Ocean between North China Block and Mongolia Block exist during the late Paleozoic? First paleomagnetic evidence from central-eastern Inner Mongolia, China, *J. Geophys. Res. Solid Earth*, *118*, 1873–1894, doi:10.1002/jgrb.50198.

1. Introduction

[2] Central-eastern Asia, located between the North China Block (NCB) and Siberia Block (SIB) (Figure 1a), is formed by long-term amalgamation of the NCB, the Mongolia Block (MOB, South Mongolia, and Amuria block), SIB, and several intermediate microcontinents [*Windley et al*., 2007]. It is considered as the southeastern part of the Altaids [*Sengör et al*., 1993], also known as the Central Asian Orogenic Belt (CAOB) in some papers [*Windley et al*., 2007; *Kröner et al*., 2010; *Xu et al*., 2012]. This area has attracted much attention from geoscientists for decades, as it represents a natural laboratory to understand accretionary processes and continental crust formation. Hence, it has been extensively studied from tectonic evolution [e.g., *Xiao et al*., 2003; *Windley et al*., 2007; *Xu et al*., 2012], geochemical and geochronological constrains [e.g., *Jahn et al*., 2009; *Litvinovsky et al*., 2011; *Wu et al*., 2011], and paleomagnetic reconstructions [e.g., *Zhao et al*., 1990; *Enkin et al*., 1992; *Pruner*, 1992; *Xu et al*., 1997; *Kravchinsky et al*., 2002a; *Cogné et al*., 2005].

[3] However, several issues dealing with the Paleozoic evolution of the Paleo-Asian Ocean between NCB and MOB are still controversial, especially the location of suture zone and the timing of the final oceanic closure. According to the unconformity between the Upper Devonian strata and the underlying rocks, and their different deformation patterns as well, *Tang* [1990] and *Xu et al*. [2012] suggested that two branches of the Paleo-Asian Ocean were closed in the Late Devonian to form two orogens between NCB and MOB, namely the North Orogen and the South Orogen (Figure 1b). These two belts are separated by a microcontinent, namely, the Hunshandake Block by *Xu et al*. [2012], referred as Inner Mongolia Block (IMB) in this paper. After that, this region underwent an extensional setting characterized by Early Permian alkine A-type granitoids and bimodal volcanic rocks [*Zhang et al*., 2008; *Jahn et al*., 2009; *Chen et al*., 2012] and extension-related sedimentation [*Tang*, 1990]. However, based on disputable geochemical interpretations, and occurrence of the Permian marine sediments, some authors

[1]Key Laboratory of Orogenic Belts and Crustal Evolution, Ministry of Education, Peking University, Beijing, China.
[2]Université d'Orléans, ISTO, UMR 7327, 45071, Orléans, France and CNRS/INSU, ISTO, UMR 7327, 45071 Orléans, France and BRGM, ISTO, UMR 7327, BP 36009, 45060 Orléans, France.

Corresponding author: B. Xu, Key Laboratory of Orogenic Belts and Crustal Evolution, Ministry of Education, Peking University, Beijing 100871, China. (bxu@pku.edu.cn)

©2013. American Geophysical Union. All Rights Reserved.
2169-9313/13/10.1002/jgrb.50198

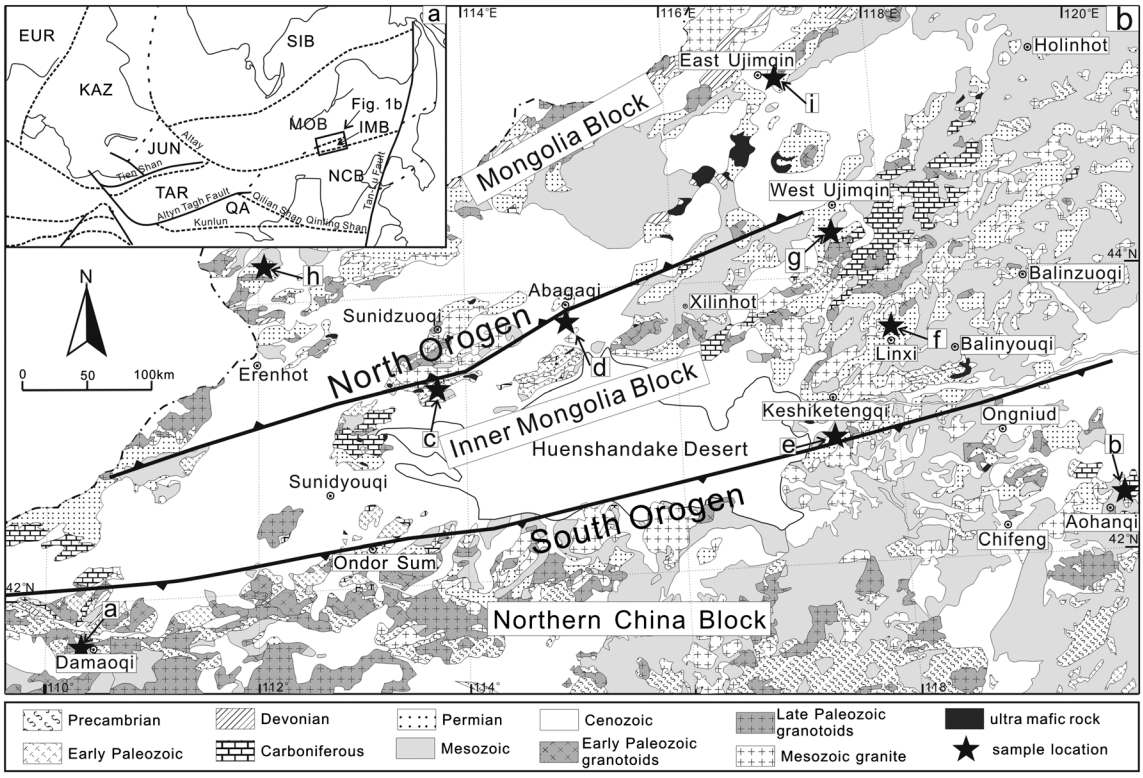


Figure 1. (a) Sketch tectonic map of Northeast Asia showing the main blocks and boundaries (modified after *Enkin et al*. [1992]). Block: EUR = Eurasia main plate; KAZ = Kazakhstan block; JUN = Junggar block; TAR = Tarim block; QA = Qaidam block; SIB = Siberia Block; MOB = Mongolia Block; NCB = North China Block. (b) Geological map of eastern Inner Mongolia emphasizing the two orogenic belts (North Orogen and South Orogen), late Paleozoic strata and intrusions (modified after *IMBGMR* [1991] and *Xu et al*. [2012]). Sampling localities: a, Damaoqi; b, Aohanqi; c, Sunidzuoqi; d, Abagaqi; e, Keshiketengqi; f, Linxi; g, West Ujimqin; h, Erenhot; i, East Ujimqin.

hypothesized that the Paleo-Asian Ocean has existed through the late Paleozoic, until the Late Permian when NCB and MOB collided [*Chen et al*., 2000; *Xiao et al*., 2003; *Johnson et al*., 2008; *Heumann et al*., 2012].

[4] Paleomagnetism is an efficient tool to study plate movements and to propose paleogeographic reconstructions. Thus, it could provide key arguments to solve the aforementioned controversy on Paleo-Asian Ocean. In East Asia, previous paleomagnetic studies have been concentrated on the study of the Mongol-Okhotsk Ocean between MOB and SIB [*Kravchinsky et al*., 2002a, 2002b; *Cogné et al*., 2005]. Conversely, paleomagnetic constraints for the Paleo-Asian Ocean remain rare and they were mostly carried out from the northern part of MOB, such as Trans-Baikal and upper Amur [*Pruner*, 1992; *Xu et al*., 1997; *Kravchinsky et al*., 2002a]. *Zhao et al*. [1990] have reported the first and only paleomagnetic study on Paleozoic rocks from Inner Mongolia; however, their results of the Late Permian (11 samples) and Carboniferous (29 samples) are clearly remagnetized with a negative fold test. Therefore, no reliable or utilizable Paleozoic paleomagnetic data are available up to now for Inner Mongolia area. For these reasons, a paleomagnetic study has been carried out on sedimentary and volcanic rocks from Paleozoic formations in central-eastern Inner Mongolia. The widespread desert and grassland hinder finding suitable outcrops for paleomagnetic sampling. It took us 3 years to investigate the area and to find all the outcrops presented in this paper.

2. Geological Setting and Paleomagnetic Sampling

2.1. Brief Geological Outline

[5] The central-eastern Inner Mongolia, located between the northern margin of the NCB and the southern margin of the MOB (Figure 1b), has recorded a complex subduction-collision history between these two continents [*Xiao et al*., 2003; *Windley et al*., 2007; *Jian et al*., 2008; *Zhang et al*., 2008; *Xu et al*., 2012]. Two well-documented ophiolitic mélange belts exposing blocks of blueschists and chert [*Xu et al*., 2001; *Xiao et al*., 2003; *De Jong et al*., 2006] are juxtaposed with two magmatic arcs, namely, the Baolidao Arc and the Bainaimiao Arc [*Chen et al*., 2000; *Jian et al*., 2008], which are located to the south of Sunidzuoqi and Ondor Sum, respectively (Figure 1b). An unconformable Late Silurian to Late Devonian molasse overlies the mélanges and postdates the early-middle Paleozoic orogenic events, recorded in the North Orogen and the South Orogen (Figure 1b) [*Tang*, 1990; *Xu et al*., 2012]. Between these two orogenic belts, a microcontinent (IMB) exposes a Precambrian basement [*Xu et al*., 2012]. In addition to the two ophiolitic mélanges, the occurrence of numerous ultramafic rocks, mainly serpentinite and metagrabbro, throughout central-eastern Inner Mongolia [*Miao et al*., 2007] led many authors to propose that they represent the ophiolitic remnants of the suture zone and to speculate that oceanic domains have persisted during the late Paleozoic [*Xiao et al*., 2003; *Li*, 2006;



Figure 2. Photographs of sampling outcrops. (a) red sandstone of S_3x in Damaoqi; (b) red sandstone of D_1c in Damaoqi; (c) limestone of C_1h in Aohanqi; (d) coarse sandstone of D_3s in Sunidzuoqi; (e) yellow siltstone of D_3s in Abagaqi; (f)coarse sandstone of P_3t in Keshiketengqi; (g) sandstone of P_3l in Linxi; (h) limestone of C_2a in West Ujimqin; (i) limestone of P_2z in West Ujimqin; (j) red sandstone of $D_{1\text{-}2}n$ in Erenhot; (k) volcaniclastic rocks of C_2-P_1g in East Ujimqin; and (i) dextral strike-slip fault observed 5 m to the right of Figure 2k position.

Miao et al., 2008]. However, the geochemical signature of most of these ultramafic rocks and their geological relationships with the surrounding units do not support an ophiolitic origin, and therefore, they do not represent a ophiolitic suture zone [*Miao et al.*, 2007; *Jian et al.*, 2012].

[6] The Precambrian basement of central-eastern Inner Mongolia is composed of the strongly deformed and metamorphosed Paleoproterozoic Baoyintu Group, and the Mesoproterozoic to Neoproterozoic Xilin Gol complex [*Inner Mongolian Bureau of Geology and Mineral Resources* (*IMBGMR*), 1991; *Xu and Chen*, 1997; *Ge et al.*, 2011]. The widespread undeformed Late Silurian and Late Devonian molassic deposits unconformably overlie the Precambrian rocks [*Xu and Chen*, 1997; *Zhang et al.*, 2010]. During the Carboniferous, IMB was covered by carbonate deposits with subordinate clastic rocks, which grade upward into Early Permian volcanic rocks, Middle Permian shallow marine deposits, and Late Permian lacustrine black mudstone-siltstone deposits [*IMBGMR*, 1991; *Mueller et al.*, 1991]. The widespread Early Permian volcanic and intrusive rocks are mostly alkaline or calc-alkaline, and the volcanic rocks present a bimodal geochemical signature, which suggest emplacement in an extensional tectonic setting [*Zhang et al.*, 2008, 2011; *Chen et al.*, 2012]. These extensional basins were closed at the end of Permian, as the Late Permian conglomerate unconformably overlying the folded Carboniferous-Permian strata. Subsequently, central-eastern Inner Mongolia experienced uplift and erosion until the deposition of Late Jurassic volcanic rocks and the formation of Early Cretaceous rift-related basins [*Meng*, 2003], associated with contemporaneous plutons intruded into the Paleozoic strata (Figure 1b).

[7] Concerning MOB, although there is no agreement for the existence of a single block, several microblocks recognized in southern Mongolia (e.g., Hutag Uul microblock and Baga Bogd massif) [*Wang et al.*, 2001; *Demoux et al.*, 2007], and in Amur area (e.g., central Mongolian, Argun, upper Amur, Khingan-Bureya blocks) [*Zonenshain et al.*, 1990] are thought to be nearby each other [*Zonenshain et al.*, 1990; *Kravchinsky et al.*, 2002a]. Meanwhile, all Paleozoic paleomagnetic results obtained on or at the margin of these microblocks display consistent paleolatitude [*Kravchinsky et al.*, 2002a and references therein], so we use MOB to represent these nearby microblocks. However, in the late Paleozoic, these microblocks may separate from each other with remnant seas, as Carboniferous arcs and marine deposits were identified [*Johnson et al.*, 2008]. The remnant seas were thought to be closed in the Late Permian, with the Permian marine succession overlain unconformably

by the Lower Triassic continental strata [*Johnson et al*., 2008; *Lehmann et al*., 2010; *Blight et al*., 2010; *Heumann et al*., 2012].

2.2. Stratigraphy of Sampled Strata

[8] The sampled strata range from Late Silurian to Late Permian, which are the key stages for studying the evolution of the eastern part of CAOB. In the following part, we describe the sampling localities using the tectonic division presented in the geological outline.

2.2.1. North Margin of NCB

[9] At the northern margin of NCB, two localities were sampled, namely Damaoqi to the west and Aohanqi to the east (localities a and b in Figure 1b, respectively).

[10] Late Silurian rocks are well defined as the Xibiehe Formation (S_3x) near Damaoqi County [*Zhang et al*., 2010]. It is composed of basal conglomerate at the bottom, grading upward into sandstone and limestone, containing corals and brachiopods, such as *Kyphophyllum*, *Progressum, syringopora*, etc. [*IMBGMR*, 1991, 2002]. Six sites of yellow sandstone with variable beddings were collected over a 500 m thick section (Figure 2a and Table 1). The Xibiehe Formation underlies the Lower Devonian Chaganhabu Formation (D_1c) with an unconformable contact. The Early Devonian assignment is based on the abundant corals, brachiopods, and bryozoans, such as *Favosites* sp. *Atrypa* sp. *Leptotrypafragilis* [*IMBGMR*, 2002]. To the north of Damaoqi, eight sites of red sandstone were collected from an about 800 m thick and gently folded section (Figure 2b and Table 1). It is worth noting that a dextral strike-slip fault showing mylonitic deformation has been identified three kilometers to the east of the sampling sites during our field work.

[11] To the north of Aohanqi County, seven sites were selected from the Lower Carboniferous Houfangshengou Formation (C_1h), which consists of thick-bedded (0.2–1 m) black limestone (Figure 2c and Table 1). This formation, more than 1200 m thick, attests for a stable platform carbonate setting. The well-preserved corals and brachiopods (*Gigantoproductus-Dibunophyllum*) constrain its Early Carboniferous age [*IMBGMR*, 1991]. Open fold without cleavage can be observed in this formation.

2.2.2. Inner Mongolia Block (IMB)

[12] Paleomagnetic samples were collected from five localities in IMB. From west to east, they are Sunidzuoqi, Abagaqi, Keshiketengqi, Linxi, and West Ujimqin (localities c, d, e, f and g, respectively, in Figure 1b).

[13] Near Sunidzuoqi and Abagaqi counties (Figure 1b), five sites of red coarse sandstone (Figure 2d) and six sites of yellow siltstone (Figure 2e) of the Upper Devonian Seribayanaobao Formation (D_3s) were collected, respectively (Table 1). The Upper Devonian Seribayanaobao Formation represents continental molasse deposits, which unconformably overlie the ophiolite mélange [*Xu and Chen*, 1997; *Xu et al*., 2012]. This formation mainly consists of red conglomerate, red-yellow sandstone, and yellow siltstone, with a top layer of argillaceous limestone. The plant fossils, such as *Leptophloeum rhombicum* in the sandstone and *Nalivkinella profunda* and *Cyrtospirifer sulcifer* in the limestone, attest to the Late Devonian age [*Xu et al*., 2012]. Near Sunidzuoqi, five sites of red sandstone were also collected from both limbs of a fold within the Lower Carboniferous Gouhuduge Formation (C_1g; Table 1), which conformably overlies the Upper Devonian strata. Open fold has been observed from Lower Carboniferous strata in the Sunidzuoqi, and the Upper Devonian strata in Abagaqi are highly tilted (Table 1).

[14] To the south of Keshiketengqi County, six sites of coarse sandstone of the Upper Permian Tieyingzi Formation (P_3t) were collected from a section with very gentile bedding (Figure 2f and Table 1). The alluvial-fluvial-lacustrine facies Tieyingzi Formation consists of conglomerate at the bottom, coarse-grained to conglomeratic sandstone in the middle, and red and green siltstone on the top. The Tieyingzi Formation unconformably overlies the Early-Middle Permian granite and the Lower-Upper Permian strata, with pebbles of all aforementioned rocks at the bottom. The enriched Late Permian plant fossils, such as *Pecopteris* sp. *Calamites* sp., *Nephropsis* sp, and the occurrence of the unconformity as well, assign the Tieyingzi Formation to the Late Permian.

[15] To the north of Linxi County, three sites of tuff and basalt from the Lower Permian Dashizhai Formation (P_1d) and three sites of sandstone from the Upper Permian Linxi Formation (P_3l) were collected (Figure 2g and Table 1). The Dashizhai Formation is composed of volcanic rocks erupted between 285 and 270 Ma, which belong to the major Late Paleozoic magmatic event widespread in Inner Mongolia [*Zhang et al*., 2008; *Liu*, 2009; *Chen et al*., 2012]. The Linxi Formation is composed of fluvial conglomerate at the bottom with pebbles of volcanic rocks of Dashizhai Formation, covered by approximately 4000 m thick black mudstone and dark yellowish siltstone/sandstone of fluvial-lacustrine facies [*Mueller et al*., 1991]. The plant fossils and fresh water bivalves, such as *Brachythyris* sp. and *Rhombotrypella* sp., and the minimum age of detrital zircons (256 ± 2Ma) [*Han et al*., 2011] well constrain its Late Permian age.

[16] To the south of West Ujimqin County, eight sites of limestone and three sites of grey fine-grained sandstone were sampled from the Upper Carboniferous Amushan Formation (C_2a; Figure 2h). As the most general Late Carboniferous deposits in Inner Mongolia, the Amushan Formation is composed of shallow marine facies carbonate and subordinate terrigeneous deposits with a well-defined age owing to enriched neritic fossils, such as *Pseudoschwagerina* and *Triticites*. To the north of West Ujimqin, five sites of yellow sandstone were sampled from both limbs of an open fold at the top of the Upper Carboniferous-Lower Permian Gegenaobao Formation (C_2-P_1g). The top sandstone of Gegenaobao Formation directly overlies volcanic rocks that have yielded a zircon concordant U-Pb age at 266 ± 2Ma (Zhao, unpublished data). Therefore, the collected sandstone is mid-Permian in age and we further use P_{2g} to represent the age for these five sites. To the south of West Ujimqin, six sites of dark blue thick-bedded limestone were collected from the middle Permian Zhesi Formation (P_2z; Figure 2i). The age determination of Zhesi Formation is based on the well-known Middle Permian Zhesi Fauna [*Wang et al*., 2004a]. The bedding attitude for the Zhesi Formation is nearly vertical, with very slight variations.

2.2.3. Southern Margin of MOB

[17] At the southern margin of MOB, two localities were chosen for paleomagnetic sampling. From west to east, they are Chaganaobao to the north of Erenhot (locality h in Figure 1b) and East-Ujimqin (locality i in Figure 1b).

Table 1. Paleomagnetic Sampling and Analysis Results From Inner Mongolia

Site	Coordinate	Rock	Age	Strike/Dip (°)	n′/n	N/R	Dg (°)	Ig (°)	Ds (°)	Is (°)	k	α_{95} (°)	Comments and Poles
					North China Block (NCB)								
Damaoqi													
1[a]	41°55′N,109°56E	red sandstone	D_1c	343.6/51.5	6/6	6/0	0.7	70.8	53.1	27.4	131.0	6.7	
2[b]	41°55′N,109°56E	red sandstone	D_1c	258.5/14	8/8	5/3	124.7	2.6	123.5	12.7	36.8	9.2	λ = 24.1°, φ = 354.2°,
3	41°55′N,109°56E	red sandstone	D_1c	210/29	6/8	6/0	29.5	55.5	354.5	45.9	49.0	9.7	dp = 4.6°, dm = 9.2°
4[b]	41°55′N,109°56E	red sandstone	D_1c	221/40	8/9	0/8	314.5	−17.2	317.1	−57.1	17.0	15.1	λ = 24.4°, φ = 340.7°, dp = 8.1°, dm = 15.6°
5	41°55′N,109°56E	red sandstone	D_1c	176/35	0/4	0/0	-	-	-	-	-	-	dispersed
6[b]	41°55′N,109°56E	red sandstone	D_1c	220.5/24	4/5	0/4	107.5	−3.6	106.0	18.5	42.0	15.1	λ = 14.2°, φ = 9.4°,
7[b]	41°55′N,109°56E	red sandstone	D_1c	179.7/42	4/6 3/4	0/4	211.7	−16.3	195.3	−35.3	594.0	4.0	dp = 7.6°, dm = 15.1° λ = 46.3°, φ = 241.1°, dp = 2.1°, dm = 4.1°
8[b]	41°55′N,109°56E	red sandstone	D_1c	190/51		0/3	235.3	−12.1	211.7	−42.2	90.0	7.1	λ = 29.5°, φ = 220.0°,
9[a]	42°00′N,110°10′E	coarse sandstone	S_3x	289/20	6/6	2/4	6.1	63.8	11.1	44.0	94.0	6.9	dp = 3.7°, dm = 7.2°
10[a]	42°00′N,110°10′E	coarse sandstone	S_3x	283.5/30	8/8	5/3	4.2	70.9	6.7	38.0	114.0	5.7	
12	42°00′N,110°10′E	coarse sandstone	S_3x	337/48	0/8	0/0	-	-	-	-	-	-	weak NRM, viscous
13[a]	42°00′N,110°10′E	greywacke	S_3x	338/49.5	7/9	4/3	5.8	66.0	44.2	26.7	21.2	13.4	
14	42°00′N,110°10′E	greywacke	S_3x	328/56	0/2	0/0	-	-	-	-	-	-	weak NRM, viscous
15	42°00′N,110°10′E	greywacke	S_3x	304/57	7/9	0/7	337.5	−9.5	314.5	−33.1	53.0	8.4	
			mean[a] (site 1, 9, 10,13)		4S/4S		3.3	67.1			635.0	3.6	λ = 81.9°, φ = 125.4°, dp = 5.0°, dm = 6.0°
									31.1	36.0	23.1	16.8	
Aohanqi													
N01[a]	42°33′N,119°47′E	limestone	C_1h	246/26	8/8	8/0	10.5	64.0	355.1	40.5	59.0	7.3	
N02[a]	42°33′N,119°47′E	limestone	C_1h	248.7/36.3	7/8	7/0	9.0	62.5	354.3	28.8	23.8	12.6	
N03[a]	42°33′N,119°47′E	limestone	C_1h	252/32.3	11/11	10/1	5.4	67.5	352.8	36.2	71.5	5.4	
N04[a]	42°33′N,119°47′E	limestone	C_1h	239/41	8/8	4/4	44.9	76.6	347.3	44.2	32.0	9.9	
N05[a]	42°33′N,119°47′E	limestone	C_1h	238.7/38.3	6/8	6/0	7.2	69.0	346.3	33.4	66.3	8.3	
N06[a]	42°33′N,119°47′E	limestone	C_1h	310/18	5/6	4/1	354.3	57.6	8.2	43.4	19.2	17.9	
N07[a]	42°33′N,119°47′E	limestone	C_1h	312.5/18.5	8/8	7/1	20.0	66.1	29.9	49.2	56.0	7.5	
			mean[a]		7S/7S		9.6	66.6			110.0	5.8	λ = 80.6°, φ = 161.9°, dp = 7.9°, dm = 9.6°
									357.8	40.0	37.8	9.9	
					Inner Mongolia Block (IMB)								
Sunidzuoqi													
O16	43°28′N,113°32′E	red coarse sandstone	D_3s	245/20	4/7	4/0	173.4	14.8	177.4	32.8	40.0	14.6	
O17	**43°28′N,113°32′E**	**red coarse sandstone**	**D_3s**	**245/20**	**6/10**	**0/6**	**164.3**	**−34.6**	**162.8**	**−15.0**	**50.0**	**11.0**	
O23	43°28′N,113°32′E	red coarse sandstone	D_3s	237/38	0/5	0/0	-	-	-	-	-	-	weak NRM, viscous
O24	**43°28′N,113°32′E**	**red coarse sandstone**	**D_3s**	**250/28**	**5/6**	**0/5**	**118.7**	**−55.6**	**131.7**	**−30.8**	**54.0**	**16.7**	
O25	**43°28′N,113°32′E**	**red coarse sandstone**	**D_3s**	**250/28**	**6/6**	**1/5**	**138.6**	**−52.8**	**143.6**	**−25.4**	**54.0**	**9.2**	
			mean		**3S/5S**		**143.6**	**−49.3**			**18.0**	**29.9**	
									144.6	**−24.3**	**24.3**	**25.5**	**λ = 46.8°, φ = 349.1°, dp = 14.6°, dm = 27.2°**
					17s/17s		**134.1**	**−49.9**			**13.0**	**10.3**	
									139.9	**−25.9**	**14.9**	**9.6**	**λ = 43.6°, φ = 356.9°, dp = 5.6°, dm = 10.4°**

Table 1. (continued)

Site	Coordinate	Rock	Age	Strike/Dip (°)	n′/n	N/R	Dg (°)	Ig (°)	Ds (°)	Is (°)	k	α_{95} (°)	Comments and Poles
O18	43°29′N,113°32′E	sandstone	C_1g	58/40	0/6	0/0	-	-	-	-	-	-	weak NRM, dispersed
O19	43°29′N,113°32′E	sandstone	C_1g	58/45	0/2	0/0	-	-	-	-	-	-	weak NRM, dispersed
O20	43°29′N,113°32′E	sandstone	C_1g	80/8	0/3	0/0	-	-	-	-	-	-	weak NRM, dispersed
O21	43°29′N,113°32′E	sandstone	C_1g	220/20	0/7	0/0	-	-	-	-	-	-	weak NRM, dispersed
O22	43°29′N,113°32′E	sandstone	C_1g	195/27	0/6	0/0	-	-	-	-	-	-	weak NRM, dispersed
Abagaqi													
25	43°56′N,114°56′E	yellow siltstone	D_3s	242.3/82.3	0/1	0/0	-	-	-	-	-	-	viscous
26	43°56′N,114°56′E	yellow siltstone	D_3s	77.5/51.5	0/1	0/0	-	-	-	-	-	-	viscous
27	43°56′N,114°56′E	yellow siltstone	D_3s	76/40	0/1	0/0	-	-	-	-	-	-	viscous
28	43°56′N,114°56′E	yellow siltstone	D_3s	72.5/53	0/1	0/0	-	-	-	-	-	-	viscous
29	43°56′N,114°56′E	yellow siltstone	D_3s	82/73.5	0/1	0/0	-	-	-	-	-	-	viscous
30	43°56′N,114°56′E	yellow siltstone	D_3s	90/62.3	0/1	0/0	-	-	-	-	-	-	viscous
Keshiketengqi													
N08 [a]	43°01′N,117°40′E	coarse sandstone	P_3t	110.7/34	5/6	5/0	350.5	63.4	252.6	73.2	220.0	5.2	
N09 [a]	43°01′N,117°40′E	coarse sandstone	P_3t	120/16.5	7/7	7/0	350.0	72.2	288.7	77.0	180.0	4.5	
N10 [a]	43°01′N,117°40′E	coarse sandstone	P_3t	136.3/17	7/7	7/0	355	68.4	306.3	73.1	208.0	4.2	
N11 [a]	43°01′N,117°40′E	coarse sandstone	P_3t	128/14	4/4	4/0	6.5	70.2	323.1	77.7	1240	3.5	
N12 [a]	43°01′N,117°40′E	coarse sandstone	P_3t	128/14	3/5	3/0	1.2	67.2	320.0	74.4	344.0	6.6	
			mean [a]		5S/5S		356.5	68.4			372.0	4.0	λ = 81.1°, φ = 103.5°, dp = 5.7°, dm = 6.7°
									297.5	76.5	114.0	7.2	
Linxi													
O01 [a]	43°43′N,118°08′E	sandstone	P_3l	332/84	9/9	9/0	6.4	73.2	134.0	18.5	269.0	3.1	
O02	43°42′N,118°25′E	tuff	P_1d	203/46	0/3	0/0	-	-	-	-	-	-	dispersed
O03	**43°42′N,118°25′E**	**basalt**	**P_1d**	**200/50**	**5/8**	**0/5**	**201.6**	**−55.1**	**148.0**	**−36.1**	**148.0**	**7.6**	
O04	**43°42′N,118°25′E**	**basalt**	**P_1d**	**200/50**	**4/7**	**0/4**	**166.5**	**−63.4**	**129.5**	**−24.8**	**138.0**	**7.8**	
O05	**43°41′N,118°17′E**	**sandstone**	**P_3l**	**210/34**	**4/4**	**4/0**	**7.8**	**57.4**	**334.7**	**38.1**	**37.4**	**17.7**	
O06	**43°41′N,118°17′E**	**sandstone**	**P_3l**	**210/34**	**8/9**	**7/1**	**347.7**	**67.3**	**326.0**	**37.4**	**95.4**	**5.7**	
West Ujimqin													
O07	44°55′N,117°27′E	sandstone	P_2g	20/65	0/4	0/0	-	-	-	-	-	-	weak NRM, viscous
O08	**44°55′N,117°28′E**	**sandstone**	**P_2g**	**12/68**	**6/8**	**0/6**	**125.9**	**−56.4**	**136.4**	**−30.4**	**35.0**	**10.0**	
O09	44°55′N,117°29′E	sandstone	P_2g	20/60	0/9	0/0	-	-	-	-	-	-	viscous
O10	**44°55′N,117°28′E**	**sandstone**	**P_2g**	**220/28**	**3/3**	**2/1**	**324.0**	**68.1**	**312.7**	**35.0**	**623.2**	**10.0**	
O11	44°55′N,117°29′E	sandstone	P_2g	225/31	0/5	0/0	-	-	-	-	-	-	dispersed
		mean Permian (site O02-O11)			**6S/10S**		**167.2**	**−63.9**			**30.4**	**12.3**	
									140.8	**−34.0**	**70.9**	**80.0**	**λ = 48.7°, φ = 3.7°, dp = 5.2°, dm = 9.1°**
O12	**45°01′N,117°18′E**	**sandstone**	**C_2a**	**277.5/67.5**	**3/3**	**0/3**	-	-	-	-	-	-	
O13	**45°01′N,117°18′E**	**sandstone**	**C_2a**	**277.5/67.5**	**5/6**	**0/5**	-	-	-	-	-	-	
O14	**45°01′N,117°18′E**	**sandstone**	**C_2a**	**275/65**	**0/1**	0/0	-	-	-	-	-	-	
			mean C_2a	**8s/10s**	**0/8**		**95.2**	**−86.4**	**178.1**	**−19.5**	**41.0**	**9.1**	

Table 1. (continued)

Site	Coordinate	Rock	Age	Strike/Dip (°)	n′/n	N/R	Dg (°)	Ig (°)	Ds (°)	Is (°)	k	α_{95} (°)	Comments and Poles
													λ = 55.0°, φ = 300.6°, dp = 5.0°, dm = 9.5°
O15	44°50′N,116°28′E	sandstone	$D_{2\text{-}4}$	352.5/12	0/5	0/0	-	-	-	-	-	-	weak NRM, viscous
N13 [a]	44°31′N,117°33′E	limestone	P_2z	86/88	3/3	3/0	-	-	-	-	-	-	
N14 [a]	44°31′N,117°33′E	limestone	P_2z	91.5/84	3/3	3/0	-	-	-	-	-	-	
N15 [a]	44°31′N,117°33′E	limestone	P_2z	93/88	2/2	2/0	-	-	-	-	-	-	
N16 [a]	44°31′N,117°33′E	limestone	P_2z	93.5/85.5	2/2	2/0	-	-	-	-	-	-	
N17 [a]	44°31′N,117°33′E	limestone	P_2z	93/85	2/2	2/0	-	-	-	-	-	-	
N18 [a]	44°31′N,117°33′E	limestone	P_2z	93/85	3/3	3/0	-	-	-	-	-	-	
			mean [a]		11s/11s		23.7	69.5			64.4	5.7	λ = 72.8°, φ = 171.5°, dp = 8.4°, dm = 9.8°
									187.9	16.3	39.6	7.3	
N19	44°15′N,117°50′E	limestone	C_2a	80/43	1/3	1/0	-	-	-	-	-	-	
N20	44°15′N,117°50′E	limestone	C_2a	80/43	3/3	3/0	-	-	-	-	-	-	
N21	44°15′N,117°50′E	limestone	C_2a	80/43	0/3	0/0	-	-	-	-	-	-	
N22	44°15′N,117°50′E	limestone	C_2a	80/43	0/3	0/0	-	-	-	-	-	-	
N23	44°15′N,117°50′E	limestone	C_2a	80/43	3/3	3/0	-	-	-	-	-	-	
N24	44°15′N,117°50′E	limestone	C_2a	80/43	3/3	3/0	-	-	-	-	-	-	
N25	44°15′N,117°50′E	limestone	C_2a	80/43	1/3	3/0	-	-	-	-	-	-	
N26	44°15′N,117°50′E	limestone	C_2a	80/43	3/3	3/0	-	-	-	-	-	-	
			mean		14s/14s		356.1	61.4	158.4	75.2	24.1	8.3	PEF
					Mongolia Block (MOB)								
Erenhot													
16	44°30′N,111°57′E	red coarse sandstone	$D_{1\text{-}2}n$	50/54	5/8	0/5	186.9	−55.9	277.3	−52.8	85.3	8.3	
17 [a]	44°30′N,111°57′E	red coarse sandstone	$D_{1\text{-}2}n$	50/54	6/8	6/0	52.8	71.3	117.6	33.0	25.5	13.5	
18	44°30′N,111°57′E	pebble	$D_{1\text{-}2}n$	50/54	0/5	0/0	-	-	-	-	-	-	dispersed
19 [a]	44°31′N,111°56′E	red coarse sandstone	$D_{1\text{-}2}n$	164/51	7/7	6/1	5.9	67.2	284.0	43.8	78.0	6.9	
20 [a]	44°31′N,111°56′E	red coarse sandstone	$D_{1\text{-}2}n$	164/51	8/8	8/0	2.1	67.8	283.1	42.4	110.0	5.3	
21 [a]	44°31′N,111°56′E	red coarse sandstone	$D_{1\text{-}2}n$	190/30	7/8	7/0	2.1	59.7	325.2	46.3	45.0	9.0	
22 [a]	44°31′N,111°56′E	red coarse sandstone	$D_{1\text{-}2}n$	177/25	4/4	4/0	345.8	62.7	311.6	50.2	143.0	7.7	
23 [a]	44°31′N,111°56′E	red coarse sandstone	$D_{1\text{-}2}n$	276/22	6/8	6/0	7.9	59.3	14.7	38.1	92.0	7.0	
24 [a]	44°31′N,111°56′E	red coarse sandstone	$D_{1\text{-}2}n$	206/77	5/5	5/0	3.1	60.7	322.8	0.6	137.0	6.6	
			mean [a]		7S/7S		5.7	65.4			89.7	5.9	λ = 85.0°, φ = 162.6°, dp = 7.8°, dm = 9.6°
									315.1	51.1	3.6	34.3	
East Ujimqin													
N27 [a]	45°22′N,116°59′E	volcanoclastic rock	C_2-P_1g	277.3/83.7	4/5	4/0	18.7	67.3	11.7	−16.3	24.5	18.9	
N28(LTC) [a]	45°22′N,116°59′E	volcanoclastic rock	C_2-P_1g	285/76.5	7/7	7/0	44.4	62.0	28.6	−11.0	40.7	9.6	
N28(HTC) [b]	45°22′N,116°59′E	volcanoclastic rock	C_2-P_1g		5/7	0/5	213.2	−17.4	225.7	54.2	89.5	10.4	λ = 43.7°, φ = 248.5°, dp = 5.6°, dm = 10.8°
N29(LTC) [a]	45°22′N,116°59′E	volcanoclastic rock	C_2-P_1g	107.5/84	4/8	4/0	52.5	46.8	167.0	39.4	54.4	12.6	
N29(HTC) [b]	45°22′N,116°59′E	volcanoclastic rock	C_2-P_1g		4/8	0/4	216.7	−22.4	330.8	−65.3	65.5	8.9	λ = 44.1°, φ = 242.5°, dp = 5.0°, dm = 9.4°
N30(LTC) [a]	45°22′N,116°59′E	volcanoclastic rock	C_2-P_1g	104/84	6/6	6/0	46.3	72.5	184.1	20.6	106.0	6.5	
N30(HTC) [b]	45°22′N,116°59′E	volcanoclastic rock	C_2-P_1g		5/6	0/5	205.2	−28.0	349.5	−65.5	100.0	8.8	λ = 52.9°, φ = 254.0°, dp = 5.3°, dm = 9.6°

Table 1. (continued)

Site	Coordinate	Rock	Age	Strike/Dip (°)	n'/n	N/R	Dg (°)	Ig (°)	Ds (°)	Is (°)	k	α_{95} (°)	Comments and Poles
N31 [a]	45°22′N,116°59′E	volcanoclastic rock	C_2-P_1g	104/84	9/9	9/0	68.6	60.8	38.2	−4.4	91.3	5.4	
N32 [a]	45°22′N,116°59′E	volcanoclastic rock	C_2-P_1g	281.5/75.5	7/7	7/0	33.0	57.0	23.5	−16.3	41.0	9.5	
			mean [a]		6S/6S		45.3	62.4			47.7	9.8	λ = 58.1°, φ = 193.4°, dp = 11.9°, dm = 15.3°
			(except three HTC)						196.7	18.1	15.5	17.6	

Sites in bold are considered to be primary remanences. Detailed discussion is in the text.
[a]Early Cretaceous remagnetized. Detailed discussion is in the text.
[b]Early Permian remagnetized. Detailed discussion is in the text.
Abbreviations. n'/ n: number of samples used to calculation/ measured sample number; N/R: normal/reversed polarity; Dg, Ig, Ds, Is: declination (D) and inclination (I) in in-situ (g) and tilt-corrected (s) coordinates; k: the best estimate of the precision parameter; $\alpha 95$: the radius that mean direction lies within 95% confidence; S, s: number of sites (S) or samples (s) used to determine pole; λ and Φ: latitude and longitude of paleomagnetic pole; dp/dm: semi-axes of the confidence ellipse of paleomagnetic pole. S3x: upper Silurian Xibiehe Formation (Fm); D1-2n and D3s: lower-middle Devonian Niqiuhe Fm and upper Devonian Seribayanaobao Fm; C1g, C1h and C2a: lower Carboniferous Gouhuduge Fm, lower Carboniferous Houfangshengou Fm, and upper Carboniferous Amushan Fm; C2-P1g: upper Carboniferou-lower Permian Gegenaobao Fm; P1d, P2z, P3l and P3t: lower Permian Dashizhai Fm, middle Permian Zhesi Fm, upper Permian Linxi and Tieyingzi Fm, respectively.

[18] To the north of Chaganaobao village, eight sites of red coarse sandstone (Figure 2j) and one site of conglomerate of the Lower-Middle Devonian Niqiuhe Formation ($D_{1\text{-}2}$n) were sampled on both limbs of the folded 4 km long profile (Table 1). The Niqiuhe Formation is composed of red conglomerate at the bottom, followed by red coarse sandstone and limestone in the middle part, and tuffecous sandstone/siltstone on the top. Corals and brachiopods fossils, such as *Leptaenopyxis bouei*, *Derbina*, and *Coelospira*, define the Early-Middle Devonian age of this formation [*IMBGMR*, 1991]. These strata were further intruded by Late Jurassic-Early Cretaceous granite and covered by contemporary volcanic rocks.

[19] Near East Ujimqin County, six sites of volcaniclastic rocks were collected from the upper part of the Upper Carboniferous-Lower Permian Gegenaobao Formation (C_2-P_1g; Figure 2k and Table 1). The Gegenaobao Formation, overlying the Late Devonian strata and granodiorite unconformably, displays conglomerate and sandstone in the lower part and volcanic breccias-andesite-rhyolite-volcanoclastic rocks in the upper part, both of which display a nearly vertical bedding attitude. The age of this formation is determined by brachiopods fossils in the clastic part, such as *Kochiproductus* sp., *Rhynchopora* sp., *Spirifer* sp. Several meters apart from the sampling sites, a W-E trending dextral strike-slip shear zone was identified (Figure 2l).

[20] For each site, six to eight cores were drilled using a portable gasoline drill. Cores were orientated by both magnetic and, if possible, solar compasses. The average differences between these two azimuths of different localities ranges between $1.5° \pm 0.5°$ and $8.0° \pm 1.4°$. When Sun measurements were not available, the average value of the locality was used to correct the orientation of the samples. Overall, about 680 cores of 86 sites were sampled from nine localities, covering most areas of central-eastern Inner Mongolia (Figure 1b and Table 1). It is worth noting that a considerable effort has been made to find all possible outcrops in this area for paleomagnetic sampling.

3. Laboratory Methods

[21] In the laboratory, cores were prepared into standard specimens with 2.5 cm in diameter and 2.2 cm in length. Before the measurements of magnetic remanence of this paleomagnetic collection, several techniques were performed to magnetic mineralogical investigation: thermal magnetic (Curie point) experiments by KLY-3S kappabridge susceptibility meter coupled with a CS3 furnace and the acquisition of isothermal remanent magnetization (IRM) by IM30 pulse magnetizer at Institut des Sciences de la Terre d'Orléans (ISTO). In order to evaluate the deformation experienced by sampled rocks, measurements of the anisotropy of the magnetic susceptibility (AMS) were also systematically performed on specimens before their demagnetization by KLY3 kappabridge susceptibility meter. The orientation of the principal magnetic fabric axes, namely, K_1, K_2, and K_3, has been measured, and the anisotropy degree (P_J) and shape parameter (T) have been calculated for each specimen as well, following *Jelínek* [1978].

[22] Usually, at least six cores were chosen from each site for demagnetization. Both thermal and alternating magnetic field techniques were carried out to progressively remove

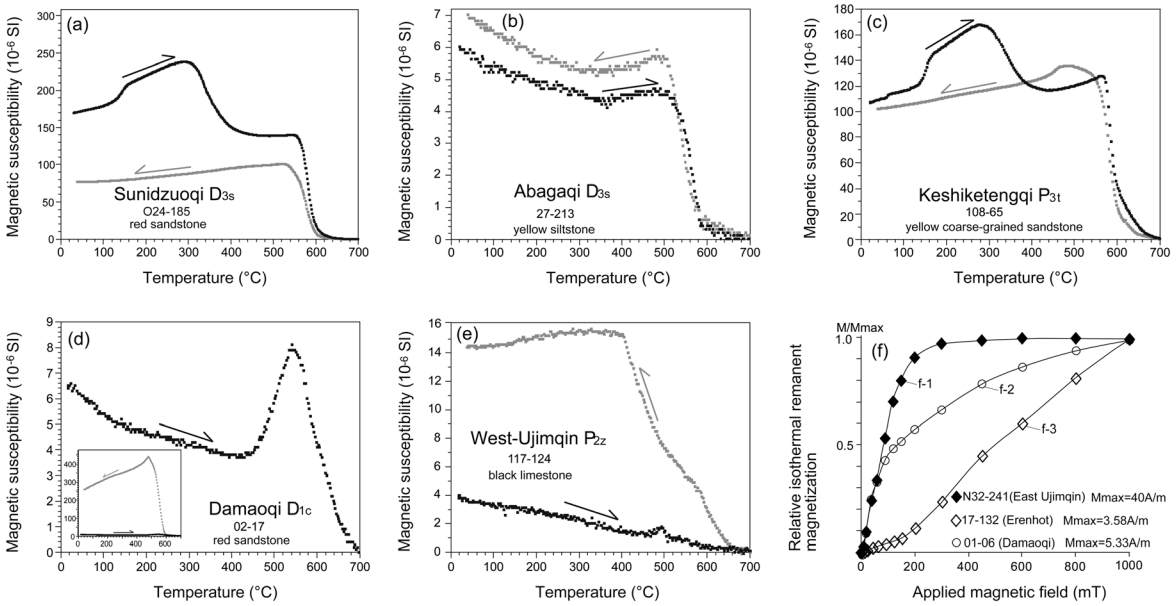


Figure 3. Representative results of (a–e) thermomagnetic experiments and (f) isothermal magnetization measurements (IRM) showing different magnetic carries. Sample name, site locality, stratigraphic age, and lithology are shown on each figure.

the magnetic remanence by about 12–16 steps with temperature intervals from 20°C to 50°C and alternating magnetic field intervals from 2 mT to 20 mT, using a laboratory-built furnace and a LDA-3 demagnetizer, respectively. Magnetic remanence was measured by JR5 magnetometer.

[23] Magnetic directions were isolated by the principal component analysis [*Kirschvink*, 1980] or estimated by great circle technique when end-points were not aligned [*McFadden and McElhinny*, 1988]. The mean magnetic directions were computed by Fisher spherical analysis [*Fisher*, 1953] using paleomagnetic software packages offered by *Cogné* [2003] and R. Enkin (unpublished).

4. Measurement Results

4.1. Magnetic Mineralogy

[24] The detailed mineralogical analyses for each locality are presented in Appendix A and summarized in the following. Three main types of magnetic carriers are identified from both thermomagnetic experiment and IRM measurement. (a) 55 out of 86 sites show magnetite is the main magnetic carrier as revealed by the sharp drop of the magnetic susceptibility at 550–585°C during thermomagnetic experiments (Figures 3a and 3b) and by the rapid increase of the IRM to a total magnetic saturation at about 300 mT (Figure 3f-1). (b) For 22 out of 86 sites, both magnetite and hematite coexist as the main magnetic carriers, deduced from the successive drops of the magnetic susceptibility from 580°C to 680°C (Figure 3c), and the relatively rapid increase of IRM at the weak applied field but without a total saturation at 1.0 T (Figure 3f-2). (c) For 9 out of 86 sites, hematite as the main magnetic carrier was indicated from the linear increase of IRM up to 1.0 T without a total saturation (Figure 3f-3), and with no drop at approximately 120°C of magnetic susceptibility, which excludes the high coercive goethite. Meanwhile, mineral transformations are common during the thermomagnetic experiments. The heating curve of Curie temperature measurements displays a rapid increase of the magnetic susceptibility at about 150°C followed by a slow increase to reach a peak at about 300°C, which may correspond to the transformation of goethite and/or pyrite into pyrrhotite and/or magnetite. In addition, the abrupt decrease from 300°C to 400°C is potentially due to maghemite destabilization (Figures 3a and 3c). For 35 out of 86 sites, heating and cooling thermomagnetic curves do not coincide, and the rapid increase of magnetic susceptibility during the cooling also indicates mineral oxidation during experiments (Figures 3d and 3e). However, it seems that mineral transformation does not disturb the thermal demagnetization, as in the majority of cases, specimens display relatively stable remanent directions.

4.2. AMS Results

[25] The AMS results for each site are presented in Appendix B. For each locality except East Ujimqin, the equal-area projection of the principal axes of the magnetic susceptibility (Figure 4a) shows nearly horizontal K_1 axes (D = 243.5°, I = 8.8°) and highly inclined K_3 axes (D = 102.5°, I = 78.8°) in tilt-corrected coordinates, which well define a horizontal magnetic fabric consistent with the initial sedimentary bedding. Meanwhile, the K_3 axes are better clustered after unfolding with the maximum/minimum radius at 95% confidence of mean K_3 axes lies at 48.5°/35.2° in in situ coordinates and 28.7°/25.6° in tilt-corrected coordinates. All samples show a relatively weak anisotropy degree with $P_J < 1.08$ (Figure 4b), suggesting that at least at the sampling scale, these rocks have not experienced intense deformation since their formation. Conversely, the data set of the volcaniclastic rocks from East Ujimqin shows well-clustered and nearly horizontal K_1, but K_3 directions are distributed along a girdle (Figure 4c). Such pattern, combining with the relatively high and heterogeneous values of P_J (Figure 4d), indicates a

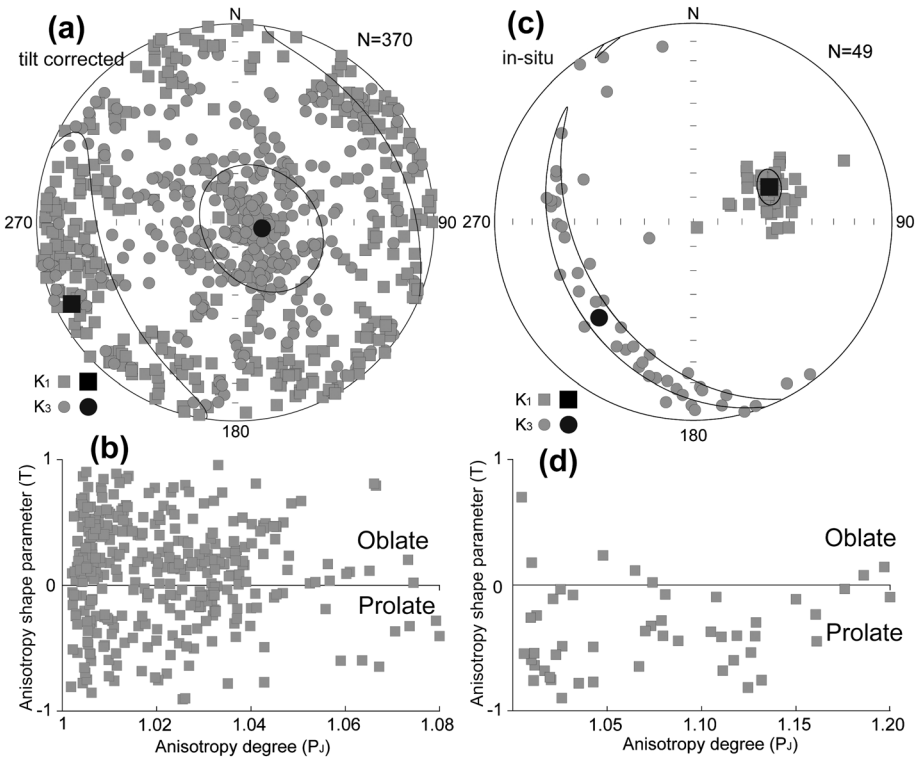


Figure 4. Results of anisotropy of magnetic susceptibility (AMS) measurements. (a and b) Equal-area stereoplot of K_1 and K_3 directions in tilt-corrected coordinates and the corresponding plots of anisotropy degree (P_J) versus anisotropy shape (T) of magnetic susceptibility for all the samples in Table B1 except sites N27–N32; (c and d) equal-area stereoplot of K_1 and K_3 directions in in situ coordinates and the corresponding plots of anisotropy degree (P_J) versus anisotropy shape (T) of magnetic susceptibility for the volcanoclastic samples from East Ujimqin (sites N27–N32) [*Jelínek*, 1978]. $P_J = \exp\{2[(\ln K_1 - \ln K_m)^2 + (\ln K_2 - \ln K_m)^2 + (\ln K_3 - \ln K_m)^2]^{1/2}\}$, and $T = 2\ln(K_2/K_3)/\ln(K_1/K_3) - 1$, where K_1, K_2, and K_3 are the maximum, intermediate, and minimum anisotropy axes, respectively.

prominent prolate shape for the fabric. This may be due to a postdeposition deformation, which is compatible with our field observation of vertical dextral strike-slip fault in the vicinity of sampling (Figure 2l). Meanwhile, both the K_1 and K_3 axes are better clustered in in situ coordinates than in tilt-corrected coordinates, suggesting that the magnetic fabric may be secondary.

4.3. Paleomagnetic Directional Analysis

4.3.1. North Margin of NCB

4.3.1.1. Damaoqi Area (S3x and D1c)

[26] The natural remanent magnetization (NRM) intensities of yellow sandstone samples of the Upper Silurian Xibiehe Formation (S_3x) are in the range of 0.25 mA/m to 38.7 mA/m. Among them, two sites (Site 12 and 14) display weak NRM (lower than 1 mA/m) and strong viscosity, and no stable paleomagnetic component can be isolated (Table 1). For others, two components were isolated from most of the samples after progressive thermal demagnetization. The low temperature component (LTC) up to 150°C displays random directions (Figures 5a and 5b). The high temperature component (HTC), isolated from 200°C to 680°C, shows two types of direction before bedding adjustments (Table 1 and Figures 5a and 5b).

[27] For the red sandstone of the Lower Devonian Chaganhebu Formation (D_1c), NRM intensities range from 1 mA/m to 202 mA/m with most of them >10 mA/m. For most of the samples, only one component was isolated from room temperature to 680°C (Table 1 and Figure 5c). In addition, few samples display two components with random low-middle temperature component (up to 500°C) and reversed HTC (Figure 5d) before tilt correction. The Enkin's direction-correction (DC) fold test [*Enkin*, 2003] is negative for this locality. Except two sites with north-northeast declination and steeply downward inclination (Sites 1 and 3) and one dispersed site (Site 5), the five remaining sites display shallow upward inclination and variable declinations ranging from 110° to 315° (Table 1).

4.3.1.2. Aohanqi Area (C1h)

[28] The NRM intensities of black limestone samples of the Lower Carboniferous Houfangshengou Formation (C_1h) range from 0.5 mA/m to 22.6 mA/m. Two components were isolated from most measured samples. After removing a dispersed viscous component up to 200°C or 2 mT, a stable component was isolated with both normal and reversed polarities before bedding adjustments (Figures 5e and 5f). A mean direction has been calculated (Table 1), which fails to pass the fold test as the directions are much better clustered before unfolding (Figure 6b).

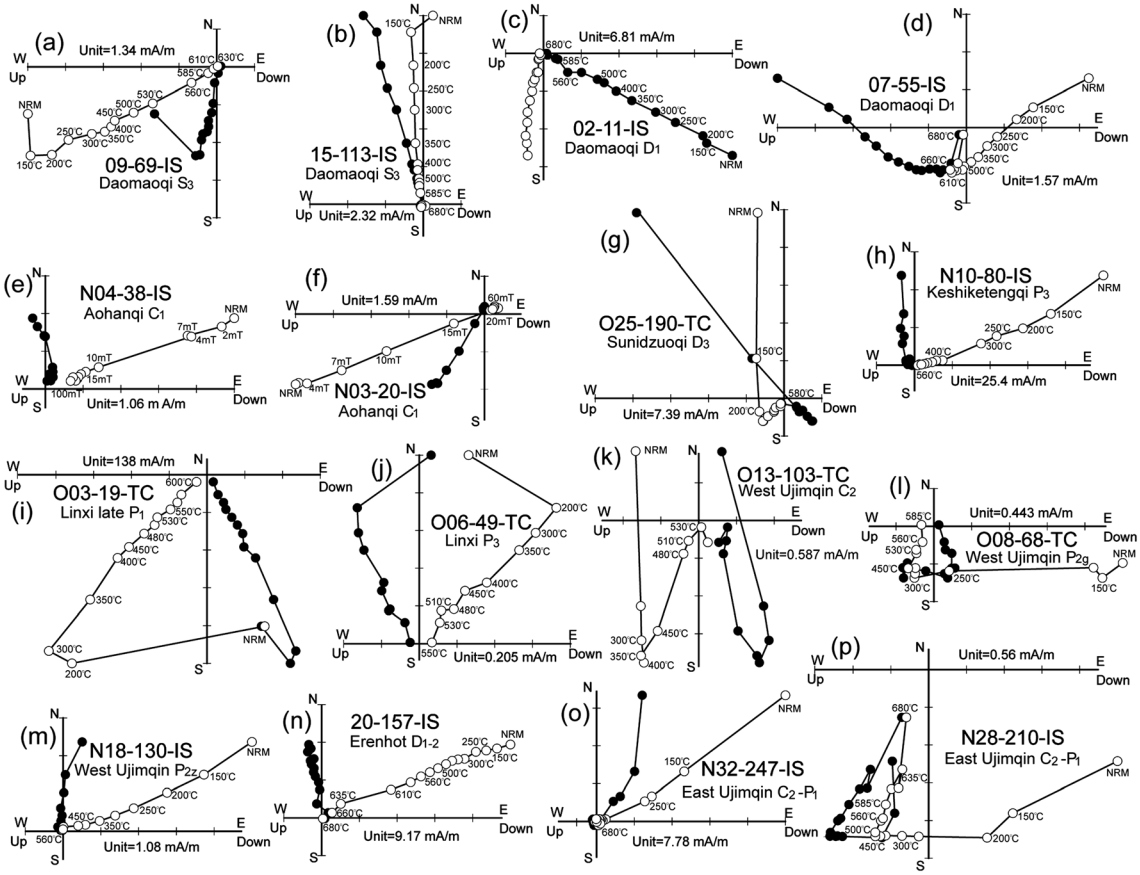


Figure 5. Orthogonal vector plots of representative specimens from each sampled age/locality group. Closed (open) symbols present the projection in horizontal (vertical) plane. IS (in situ) and TC (tilt-corrected) stands for plot in in situ and tilt-corrected coordinates. Sample name, site locality, and stratigraphic age are shown on each figure.

4.3.2. Inner Mongolia Block

4.3.2.1. Sunidzuoqi Area (D3s)

[29] For the red coarse sandstone of the Upper Devonian Seribayanaobao Formation (D_{3s}), two components of magnetic directions have been isolated from four out of five sites. The LTC is characterized by prominently viscous and dispersed directions (Figure 5g). After cleaning this viscous magnetic remanence up to 250°C, three sites (O17, O24, and O25) display a uniform reversed polarity in tilt-corrected coordinates, except one sample in Site O25 presents antipodal normal polarity (Figure 5g and Table 1). Site O16 presents normal polarity, which is much different from other sites. Therefore, we have calculated a mean direction for these three sites (Table 1). The fold test is inconclusive but the directions are better clustered after unfolding (Figure 6c). All five Lower Carboniferous sites (sites O18 to O22) show weak NRM intensity ranging from 0.25 mA/m to 5.94 mA/m or high viscosity, with no reliable direction obtained (Table 1).

4.3.2.2. Abagaqi Area (D3s)

[30] For the yellow siltstone of the Upper Devonian Seribayanaobao Formation, all specimens present weak NRM values with a range of 0.41 mA/m to 3.69 mA/m. Furthermore, most samples present highly viscous features during demagnetization, since we observe a more than 90% drop of the magnetic intensity after heating up to 150°C. Consequently, no reliable direction was isolated from this locality.

4.3.2.3. Keshiketengqi Area (P3t)

[31] For the coarse sandstone of the Upper Permian Tieyingzi Formation, the NRM intensities are relatively high, ranging from 46.4 mA/m to 227 mA/m. Only one component has been isolated from all analyzed samples (Figure 5h), and a mean direction has been calculated for these five sites (Table 1). The site mean directions are better clustered before bedding corrections, indicating a negative fold test (Figure 6d).

4.3.2.4. Linxi Area (Late P1d and P3l)

[32] For the upper part of the tuff and basalt of the Lower Permian Dashizhai Formation (P_1d), NRM intensities vary from 1.91 mA/m to 1.89 A/m. By thermal demagnetization, a random LTC has been isolated below 300°C. Thereafter, a HTC up to about 600°C has been observed and displays southeastward declination and upward inclination in tilt-corrected coordinates (Figure 5i).

[33] Concerning the sandstone of the Upper Permian Linxi Formation (P_3l), after removing the LTC until about 200°C, the remanent magnetization shows a stable decrease of magnetic remanence up to 550°C. All samples except one display unified normal polarity (Table 1). Site O01 displays northward declination and steeply downward inclination in in situ coordinates (Table 1). The tilt-corrected directions

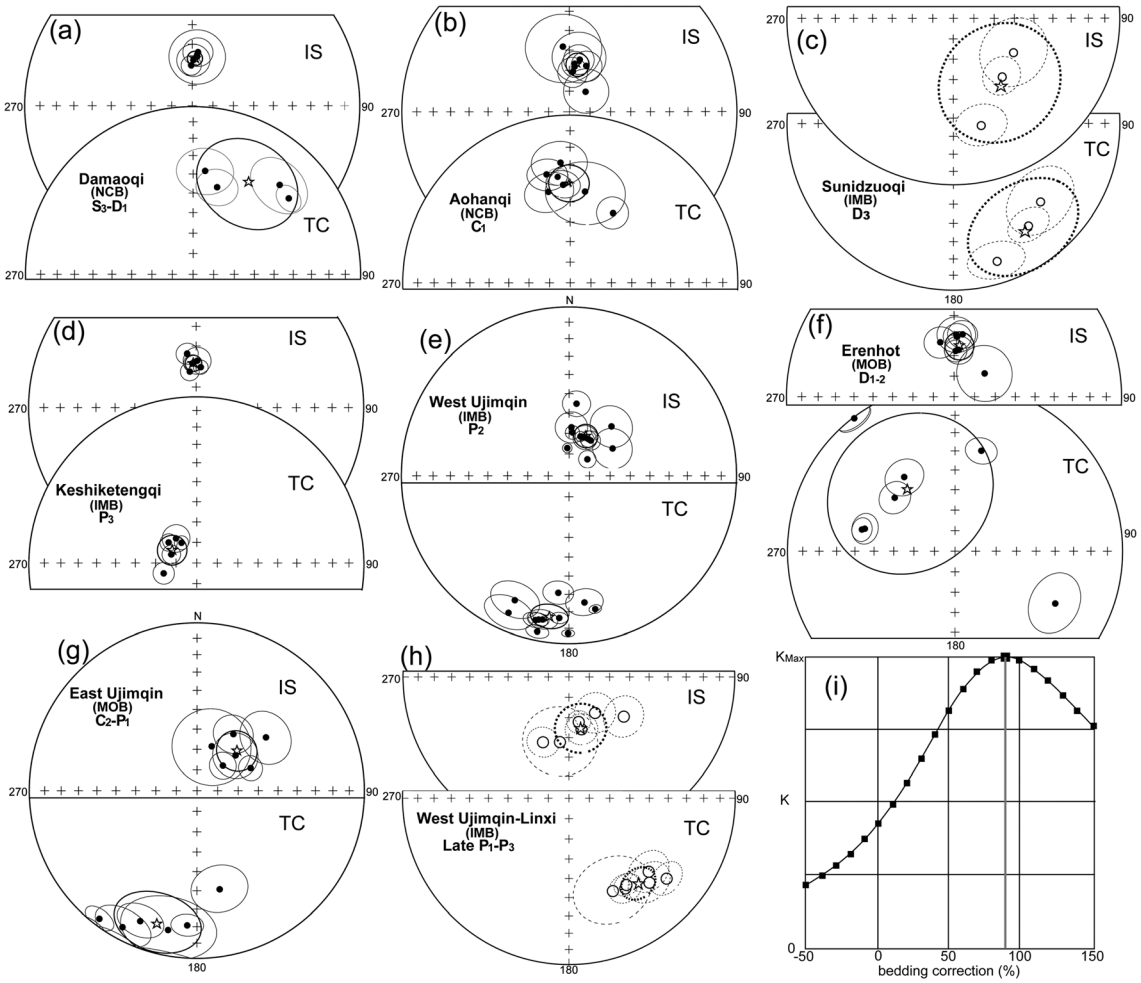


Figure 6. (a–h) Equal-area projection plots of site-mean directions of studied localities (data from Table 1). Closed (open) symbols present downward (upward) magnetic directions. Star symbols present the mean directions. IS (TC) stands for in situ/geographic (tilt-corrected/ stratigraphic) coordinates. (i) *Enkin* [2003] DC fold test: progressive unfolding showing a significant clustering of magnetic directions after bedding corrections at 90% untilting for the six Permian sites from West Ujimqin-Linxi area showing in Figure 6h.

for the other two sites display consistent northwestward declination and downward inclinations (Figure 5j).

4.3.2.5. West Ujimqin Area (C2a, P2g, and P2z)

[34] For the limestone of the Upper Carboniferous Amushan Formation (C_2a), after removing the random LTC until 200°C, all samples show normal polarity before bedding correction and a mean direction has been calculated (Table 1), which is close to that of the Present Earth Field (PEF: D = −4.3°, I = 61.2°) or Geocentric Axial Dipole (GAD: D = 0°, I = 62.2°) for the sampling area. Only eight specimens from three sandstone sites of Amushan Formation were successfully demagnetized and all display reversed polarity (Figure 5k), and a mean direction has been calculated (Table 1).

[35] For the Middle Permian yellow sandstone of the Gegenaobao Formation (P_2g), most of the samples display weak values of NRM (lower than 1 mA/m) and no reliable direction has been obtained except for Sites O08 and O10 (Table 1). For specimens of site O08, after removing the viscous LTC up to about 300°C, the remanent magnetization decreases linearly to the origin at 585°C, with solo reversed polarity (Figure 5l), while Site O10 displays antipodal normal and reversed polarities (Table 1).

[36] For the limestone of the Middle Permian Zhesi Formation (P_2z), after cleaning the LTC up to 150°C, all measured samples show consistent directions (Figure 5m) before bedding corrections and a mean direction has been calculated (Table 1). The directions are better clustered before bedding correction (Figure 6e), indicating a negative fold test.

4.3.3. South Margin of MOB

4.3.3.1. Erenhot Area (D1-2n)

[37] For the red coarse sandstone of the Lower-Middle Devonian Niqiuhe Formation ($D_{1\text{-}2}n$), only one component is isolated after progressive demagnetization, but samples from these nine sites display variable directions. Site 16 yields magnetic directions of reversed polarity. Site 18, which was selected for conglomerate test, displays scattered directions. All other seven sites, except one sample from Site 19, display a consistent normal polarity in in situ coordinates (Figures 5n and 6f) and a mean direction has been calculated (Table 1). Although the pebbles give scattered directions, the site mean directions are better grouped before tilt correction, suggesting a negative fold test (Figure 6f).

4.3.3.2. East Ujimqin (C2-P1g)

[38] For the volcanoclastic rocks of the Upper Carboniferous-Lower Permian Gegenaobao Formation (C_2-P_1g), only one component has been isolated from three sites (Sites N27, N31 and N32), and two components have been isolated from the other three (Sites N28, N29, and N30). The directions from three single-component sites are consistent with that of the LTC deduced from the three dual-component sites (Figures 5o and 5p) and a mean direction has been calculated (Table 1). The site mean directions of these six sites are better grouped before tilt correction, indicating a negative fold test (Figure 6g). The HTC isolated from three dual-component sites displays a solo reversed polarity (Figure 5p). The site mean directions for these three sites are better grouped before bedding correction, also indicating a negative fold test.

5. Discussion

[39] Magnetic mineralogy studies reveal that titanium-poor magnetite and sometimes hematite are the main magnetic remanent carrier with subordinate magnetic minerals, such as goethite, pyrrhotite, and maghemite. AMS measurements suggest that all collected rocks, except those from East Ujimqin, have not experienced intense deformation since their formation and maintain their original sedimentary magnetic fabric. Seventeen out of the 86 analyzed sites present either too weak magnetic remanent intensity or strong viscosity (Table 1) to provide reliable paleomagnetic directions. Besides, for four sites, specimens display scattered directions that hinder calculation of the site mean direction. All these 21 sites are rejected for further discussion.

5.1. Calculations of Paleomagnetic Poles

5.1.1. Primary Magnetizations

[40] Three Late Devonian sites from Sunidzuoqi show a unified reversed polarity, except one sample in Site O25 displaying an antipodal normal polarity (Table 1). Although the fold test is inconclusive due to probably the similarity of bedding attitudes, the features that the precision parameter has been improved after bedding corrections with a ratio of 1.35 for k_s/k_g and the coexistence of antipodal normal and reversed polarities may suggest that the magnetic remanence was at least acquired before the folding. The folding age cannot be, however, estimated by local stratigraphic contacts. At the regional scale, the Upper Devonian-Upper Permian strata are folded or highly tilted, and unconformably covered by the Late Permian conglomerate. Therefore, the folding took place during the Late Permian. Meanwhile, the coexistence of antipodal normal and reversed polarities and inexistence of the Early Permian magmatic rocks around sampling places exclude the Early Permian remagnetization, which displays only reversed polarity due to the Permo-Carboniferous Reversed Superchron (PCRS), ranging from 320 Ma to 263 Ma [*Garcia et al*., 2006; *Cottrell et al*., 2008]. Thus, the magnetic remanence may be considered as primary and a Late Devonian paleomagnetic pole has consequently been calculated for IMB at $\lambda = 46.8°$N, $\varphi = 349.1°$E, dp = 14.6, dm = 27.3 with N = 3 sites, or $\lambda = 43.6°$N, $\varphi = 356.9°$E, dp = 5.6, dm = 10.4 with N = 17 samples (Table 1).

[41] Only eight specimens were successfully demagnetized from three sites of Late Carboniferous sandstone from West Ujimqin, displaying a unified reversed polarity. The corresponding pole was calculated at $\lambda = 55°$N, $\varphi = 300.6°$E, dp = 5°, dm = 9.5° with paleolatitude of ~10° (Table 1). The solo reversed polarity seems to be consistent with the PCRS. The pole and the paleolatitude are comparable with the Late Carboniferous pole from Hexi Corridor in the westernmost part of NCB ($\lambda = 58°$N, $\varphi = 262.5°$E, dp = 7.4°, dm = 14.2°) [*Wu et al*., 1993] and its paleolatitude (9.2°N ± 7.4°N given by *Wu et al*. [1993] and 5.4°N given by *Huang et al*. [2001]). Although no fold test can be applied because of the small amount of samples, it seems reasonable to consider this pole to be representative of IMB for Late Carboniferous. However, for cautious tectonic interpretation, we will not use this pole further.

[42] Two sites of Early Permian basalt and two sites of Late Permian sandstone from Linxi and two sites of Middle Permian sandstone from West Ujimqin display similar or antipodal directions after bedding corrections (Figures 5i, 5l, and 5j). Zircon U-Pb geochronology yielded ages ranging between 285 Ma and 270 Ma for the basalt sites [*Zhang et al*., 2008; *Liu*, 2009]. Our unpublished zircon U-Pb dating provides a Middle Permian age assignment for the sandstone from West Ujimqin, which overlies the basalt directly. In addition, the solo reversed polarity suggests that the magnetic remanence has been acquired before 263 Ma, which is the upper limit of PCRS. Similarly, the age of the Linxi Formation sandstone is well constrained by abundant plant fossils and detrital zircon geochronology (256 Ma for the youngest grain) [*Han et al*., 2011]. Meanwhile, its chiefly normal polarity may suggest that the magnetic remanence was acquired shortly after 263 Ma, the upper limit of PCRS. All these rocks were deposited during a period of ca. 30 Ma, but they display similar or antipodal magnetic directions (Figures 5i, 5j, and 5l). This indicates a relatively stable paleolatitude for IMB from late Early Permian to Late Permian. Therefore, we have calculated a mean direction for these six sites at $D_g = 167.2°$, $I_g = -63.9°$, $k_g = 30.4$, $\alpha_{95g} = 12.3°$ and $D_s = 140.8°$, $I_s = -34.0°$, $k_s = 70.9$, $\alpha_{95s} = 8.0°$ (Figure 6h and Table 1). Enkin's fold test is positive with maximum value of k parameter at 90% (Figures 6h and 6i), and it also passes the reversal test [*McFadden and McElhinny*, 1990], suggesting that the magnetic remanences were obtained before folding. As discussed above, the folding age is considered to be the Late Permian. Therefore, we consider that the remanences were acquired during deposition. Thus, a late Early Permian-Late Permian paleomagnetic pole has been calculated for IMB at $\lambda = 48.7°$N, $\varphi = 3.7°$E, dp = 5.2°, dm = 9.1° with N = 6 (Table 1).

5.1.2. Secondary Magnetizations

[43] All other 54 remaining sites (including the Late Silurian and Early Devonian of Damaoqi, Early Carboniferous of Aohanqi, Late Permian-Early Triassic of Keshiketengqi, Late Carboniferous and Middle Permian of West-Ujimqin, Early-Middle Devonian of Erenhot, and Late Carboniferous-Early Permian of East-Ujimqin) fail to pass the fold test, suggesting post-folding remagnetizations. Two groups of directions have been identified: (a) southward (southeastward and southwestward) declinations and shallow upward inclinations (Figures 5c, 5d, and 5p) and (b) northward declinations and steeply downward inclinations or antipodal southward declinations and steeply upward inclinations (Figures 5f, 5h, 5m, and 5n). In the following, we will discuss the possible reasons and age for these remagnetizations.

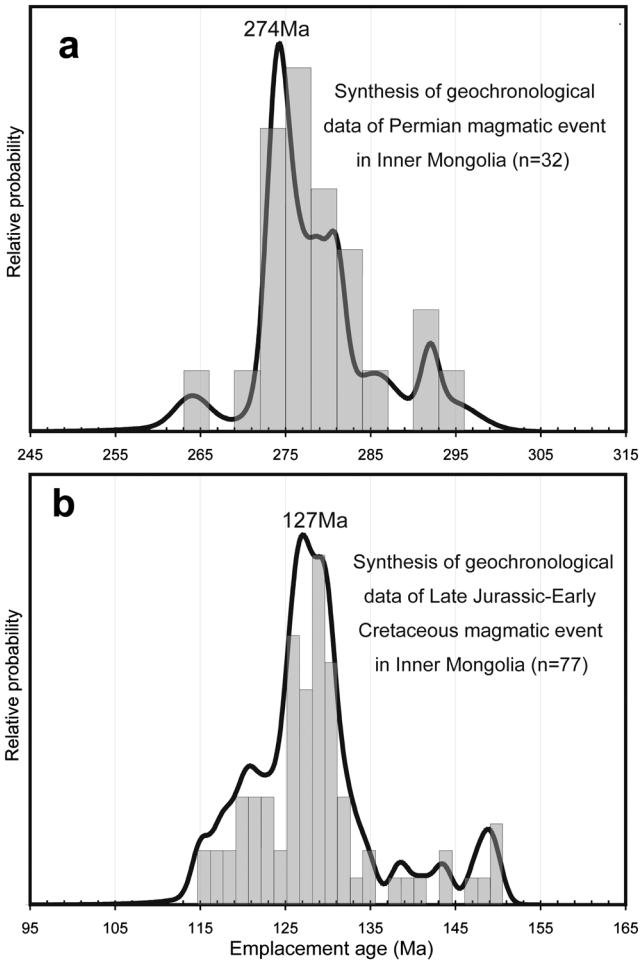


Figure 7. (a) Synthesis of geochronological data of the Permian magmatic event around Damaoqi and East Ujimqin (n = 32), illustrating the activity peak at 274 Ma, which may be responsible for the Early Permian remagnetization in these two localities. Individual data are from *Zhang et al*. [2008], *Liu* [2009], *Luo et al*. [2009], *Zhao et al*. [2011], and *Chen et al*. [2012]. (b) Synthesis of geochronological data of the Late Jurassic-Early Cretaceous magmatic event in Inner Mongolia and southern Mongolia, showing the activity peak at 127 Ma (n = 77), which may be responsible for the Early Cretaceous widespread remagnetization in Inner Mongolia. Individual data are from *Liu et al*. [2005], *Wu et al*. [2005], *Wei et al*. [2012], and *Daoudene et al*. [2012].

[44] The directions of HTC of five sites from the Early Devonian red sandstone in Damaoqi (D_{1c}) and of three sites from volcanoclastic rocks in East Ujimqin (C_2-P_1g) show the solo reversed polarity (Table 1). Moreover, these sites are close to Early Permian granitic plutons and volcanic rocks, which could be the cause of this secondary thermal magnetization. In addition, a review of the literatures concerning Permian magmatism around these two localities has shown a peak emplacement age at ca. 274 Ma (Figure 7a) [*Zhang et al*., 2008; *Liu et al*., 2009; *Chen et al*., 2012]. The solo reversed polarity and the estimated age of this remagnetization coincide with timing and features of the PCRS. Among these sites, inclinations vary slightly (−5° to −28°), but the corresponding paleolatitudes remain similar. Conversely, declinations are scattered and vary between 110° and 315° (Table 1). The paleomagnetic poles calculated from each site are distributed along a small circle centered at the sampling zone, which overlaps with Permian poles obtained from NCB and MOB (Figure 8b). So it is reasonable to consider that the remagnetized remanence acquired during the Early Permian. The important difference in declination may be due to posterior late strike-slip faulting, as observed in the field (Figure 2l).

[45] All remaining remagnetized sites display HTC directions close to that of the PEF (Table 1), but two major features allow us to distinguish them (except eight sites of Late Carboniferous limestone in West Ujimqin) from that of PEF: (1) the magnetic inclinations (62.4° to 69.5°) are higher than that of PEF (61.2° for PDF and 62.2° for GAD) and (2) the occurrence of reversed polarity for each locality (e.g., Figures 5a and 5f and Table 1). Therefore, the remagnetization age needs to be estimated. The corresponding poles of these remagnetized sites are compatible with the Early Cretaceous poles of NCB, MOB, and SIB [*Halim et al*., 1998; *Kravchinsky et al*., 2002b; *Cogné et al*., 2005; *Charles et al*., 2011]. Meanwhile, East Asia, including MOB, IMB, and NCB, experienced Mesozoic extensional tectonics, characterized by abundant extensional half-graben basins and emplacement of numerous magmatic massifs [e.g., *Webb et al*., 1999; *Graham et al*., 2001; *Ren et al*., 2002; *Liu et al*., 2005; *Wu et al*., 2005; *Charles et al*., 2011; *Wei et al*., 2012; *Daoudene et al*., 2012]. The magmatic event, which may induce thermal remagnetization, started in Late Jurassic and reached the peak in the Early Cretaceous (127 Ma, Figure 7b). After the Early Cretaceous, no magmatic event occurred in central-eastern Inner Mongolia until the early Pleistocene basalt erupted nearby Xilinhot [*IMBGMR*, 1991]. However, the distribution of the Early Pleistocene basalt is restricted, and the magnetic directions of the Early Pleistocene in this area are different from our remagnetized directions [*Zhu et al*., 1998]. Generally speaking, pervasive remagnetization is caused by regional magmatic event. So it is reasonable to consider that these secondary thermal magnetizations were acquired in Early Cretaceous.

5.2. Comparisons of the Paleomagnetic Poles

[46] Up to now, no reliable Paleozoic paleomagnetic data have been documented from central-eastern Inner Mongolia, except a few remagnetization data obtained from Carboniferous-Permian strata in northeastern Inner Mongolia [*Zhao et al*., 1990]. For MOB, paleomagnetic studies have mostly focused on its northern margin, such as North Amuria [*Xu et al*., 1997; *Kravchinsky et al*., 2002a] and North Mongolia [*Pruner*, 1987], with a few studies on South Mongolia [*Pruner*, 1987]. Most of these data were driven from deformed zones, e.g., the suspected Mongol-Okhotsk suture zone, where the strike-slip movements may have caused significant deflection of the paleomagnetic directions [*Kravchinsky et al*., 2002a; *Webb and Johnson*, 2006; *Webb et al*., 2010; *Metelkin et al*., 2010].

5.2.1. Late Devonian

[47] Late Devonian poles for these four blocks remain rare. For NCB, two poles were obtained from the Hexi Corridor region. *Zhao et al*. [1993] gave a Late Devonian pole at λ = 34.2°N, φ = 228.7°E, A_{95} = 8.8° with 16 sites of red sandstone and andesite (Table 2). *Huang et al*. [2000] calculated a mean Middle-Late Devonian pole at λ = 56°N, φ = 336°E, A_{95} = 9.2° with 12 sites of Middle-Late

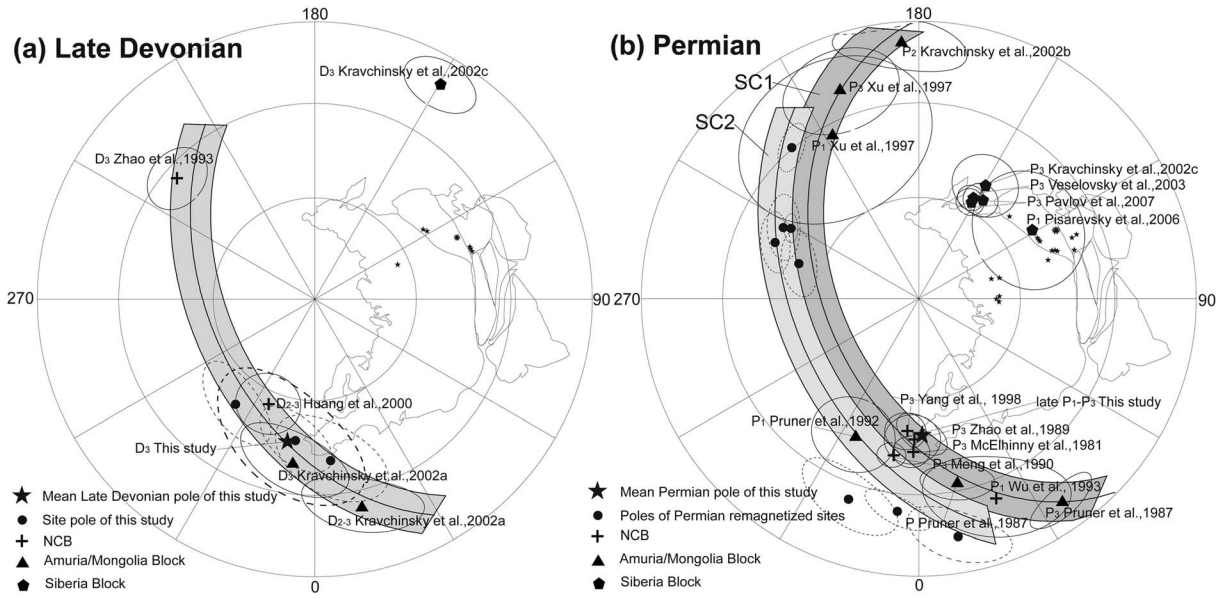


Figure 8. (a) Equal-area projections of Late Devonian poles from Sunidzuoqi (IMB), North China Block (NCB), Mongolia Block (MOB), and Siberia Block (SIB). There is little or no latitudinal difference but huge longitudinal differences between IMB, NCB, and MOB, indicating that these three blocks probably aggregated together, but with strong rotation. SIB was far away from other three blocks in Late Devonian as the pole was far away. (b) Equal-area projections of Permian poles from IMB, NCB, MOB, and SIB. The pole of our study is consistent with that of NCB, suggesting that these two parts have been welded as a rigid block. There is no latitudinal difference but still huge longitudinal differences between IMB + NCB and MOB, indicating strong postdated rotation, probably due to intracontinental strike-slip movements. SIB was still far away from other three blocks in Permian. The Permian remagnetized sites are also aligned along a small circle (SC2) with a shallower inclination, which probably due to local deformation since samples were collected from zones where strike-slip faults are documented.

Devonian strata (Table 2). Despite collecting in close locations less than 40 km, these two poles display huge rotation with declination difference of $72.1° \pm 15.4°$ (Figure 8a), which is probably caused by the strike-slip fault system in the Hexi Corridor [*Huang et al*., 2000]. In the upper Amuria region (MOB), *Kravchinsky et al*. [2002a] obtained two poles for Middle-Late Devonian and Late Devonian ages at $\lambda = 24.6°$N, $\varphi = 12.9°$E, $dp = 8.7°$, $dm = 16.9°$ with seven sites of siltstone and tuff and $\lambda = 40.5°$N, $\varphi = 352.4°$E, $dp = 9°$, $dm = 16.7°$ with five sites of sandstone and siltstone, respectively (Table 2). All these four Devonian poles from NCB and MOB are distributed along a small circle, indicating that these two blocks have evolved together without detectable paleolatitude difference ($2.3° \pm 5.7°$), but with significant relative rotations since the Late Devonian (Figure 8a). Our Late Devonian pole obtained from Sunidzuoqi (IMB) also locates on this small circle (Figure 8a), indicating that these three blocks of compatible paleolatitudes were juxtaposed since at least Late Devonian. Based on a paleomagnetic study of kimberlite and dyke in the east of Siberia, *Kravchinsky et al*. [2002c] gave a Late Devonian pole for SIB at $\lambda = 11.1°$N, $\varphi = 149.7°$E, $A_{95} = 8.9°$ with 11 localities (Table 2). This pole is totally different from the Late Devonian poles of NCB, MOB, and IMB (Figure 8a), indicating that SIB was located far away from NCB, MOB, and IMB during the Late Devonian.

5.2.2. Permian

[48] The Permian poles for NCB have been well documented by numerous studies over the last three decades (Table 2) [e.g., *McElhinny et al*., 1981; *Zhao and Coe*, 1989; *Meng et al*., 1990; *Wu et al*., 1993; *Yang et al*., 1998]. These poles are well consistent with each other (Figure 8b). Although statistically distinguished from other poles, the pole from Hexi Corridor (Figure 8b) [*Wu et al*., 1993] presents a compatible paleolatitude, indicating post-Permian rotation of sampling area with respect to the other parts of NCB.

[49] Our primary Permian pole for IMB inferred from West Ujimqin-Linxi (star in Figure 8b) is well consistent with the poles of NCB, with an indistinguishable angular difference of $2.6° \pm 10.9°$ and a weakly paleolatitudinal difference of $5.8° \pm 8.5°$ comparing with the mean Permian pole of NCB (calculated at $\lambda = 46.0°$N, $\varphi = 355.2°$E, $A_{95} = 4.7°$), indicating that no paleomagnetically detectable relative movement has occurred between NCB and IMB during Permian. These two blocks may have been welded as a rigid block.

[50] The Permian poles of MOB are distributed along a small circle, which intercepts the poles of NCB-IMB (SC1 in Figure 8b) [*Xu et al*., 1997; *Kravchinsky et al*., 2002b; *Pruner*, 1987, 1992]. This observation indicates that the post-Permian relative movements between NCB-IMB and MOB are essentially produced by rotations within these blocks. In fact, as described before, the samples of MOB come essentially from the marginal zones [e.g., *Kravchinsky et al*., 2002b]. These significant relative rotations may be caused by strike-slip movements along the tectonic boundaries [*Cogné et al*., 2005; *Metelkin et al*., 2010].

Table 2. Compilation of Late Devonian and Permian Palaeomagnetic Data of North China Block, Inner Mongolia Block, Mongolia Block and Siberia Block[a]

Age	Slat (°N)	Slong (°E)	N	Plat (°N)	Plong (°E)	A_{95}(°) (dp/dm)	Test	References
				North China Block (NCB)				
P_2	39.6	98.0	33S	42.4	350.9	3.9	F	*Meng et al.* [1990]
P_2			11L	50.3	355.2	5.7	F	*Yang et al.* [1998]
P_2	37.8	112.3	12S	44.0	358.0	6.9	F	*McElhinny et al.* [1981]
P_2	37.5	114.4	4S	47.1	356.9	7.7	F	*Zhao and Coe* [1989]
P_1	37.6	101.3	5S	23.9	21.2	12.8/21.4	F	*Wu et al.* [1993]
D_3	37.4	105.7	16S	34.2	228.7	8.8	F, R	*Zhao et al.* [1993]
D_{2-3}	37.7	106.0	14S	56.0	336.0	9.2	F, R	*Huang et al.* [2000]
				Inner Mongolia Block (IMB)				
Late P_1-P_3	43.7	118.4	6S	48.7	3.7	5.2/9.1	F	This study
D_3	43.5	113.5	3S	46.8	349.1	14.6/27.3	-	This study
				Mongolia Block (MOB)				
P_3	48.1	105.9	27s	11.3	35.2	5.4/9.1	F	*Pruner* [1987]
P_3	51.5	115.4	14S	20.5	200.6	14.5	F	*Xu et al.* [1997]
P_2	50.6	116.9	14S	8.3	183.9	9.5/16.2	F	*Kravchinsky et al.* [2002b]
P_1	51.5	115.4	5S	33.8	207.8	26.3	F	*Xu et al.* [1997]
P_1	47.8	107.1	4S	44.8	335.1	11.6	F	*Pruner* [1992]
P	48.3	106.0	52s	32.8	11.8	5.8/9.9	F	*Pruner* [1987]
D_3	54.0	123.5	5S	40.5	352.4	9.0/16.7	F, R	*Kravchinsky et al.* [2002a]
D_{2-3}	54.0	123.5	7S	24.6	12.9	8.7/16.9	F, R	*Kravchinsky et al.* [2002a]
				Siberia Block (SIB)				
P_3	64.6	114.7	9L	50.8	149.6	9.4	-	*Kravchinsky et al.* [2002c]
P_3			7L	56.2	151.7	3.8	-	*Veselovsky et al.* [2003]
P_3	67.5	104.0	8S	55.1	147.0	5.0	-	*Pavlov et al.* [2007]
P_3	67.0	89.0	8S	57.2	151.1	4.0	-	*Pavlov et al.* [2007]
P_2	50.8	107.2	15S	63.1	151.0	13.5/15.0	F	*Kravchinsky et al.* [2002b]
P_1	51.7	104.1	5S	50.5	121.4	16.9	BC	*Pisarevsky et al.* [2006]
D_3	64.0	116.0	11L	11.1	149.7	8.9	-	*Kravchinsky et al.* [2002c]

[a]Abbreviations. N: the number of sites (S), samples (s) or localities (L) used for calculation. The "S" means several sites in a relatively constrained locality; while the "L" represents a mean pole calculated from several localities, with several sites in each locality; Slat (Plat): the latitude of sampling site (pole); Slong (Plong): the longitude of sampling site (pole); A95: the radius that mean pole lies within 95% confidence, in degree; dp/dm: semi-axes of the confidence ellipse of palaeomagnetic pole; F: fold test; R: reversal test; BC: baked contact test.

[51] The Early Permian remagnetized poles obtained from Damaoqi in the northern margin of NCB and from East Ujimqin in the southern margin of MOB are scattered, but once again, they are distributed along a small circle (SC2 in Figure 8b), revealing importance of strike-slip tectonics. Though both of these two small circles are overlapped (Figure 8b), the SC2 seems slightly shallower than SC1 that intercepts all other poles from NCB, IMB, and MOB. This slight latitudinal difference between SC1 and SC2 may be due to (1) the uncertainty in age estimation for the remagnetization made by the correlation with the regional peak of magmatic activity around the sampling area and (2) the uncertainty in bedding corrections of Permian remagnetized data. As multiphase tectonic events took place after the Early Permian remagnetization, the in situ Permian remagnetized data may also consequently introduce errors in the paleolatitudes.

[52] The Permian poles from Siberia are statistically grouped [*Kravchinsky et al.*, 2002c; *Veselovsky et al.*, 2003; *Pavlov et al.*, 2007], except an outlier obtained from mafic dykes (Figure 8b) [*Pisarevsky et al.*, 2006]. These poles are far away from all other poles of NCB, IMB, and MOB, indicating that significantly latitudinal movements have occurred since Permian between Siberia and other blocks.

5.3. Tectonic Implications

[53] As a major tectonic implication of this study, no obvious latitudinal differences between IMB, NCB, and MOB are observed neither in Late Devonian nor in the Permian (Figures 8a and 8b), indicating that these three blocks have been amalgamated since the Late Devonian and no wide ocean existed between them during the Late Paleozoic. This observation is compatible with the tectonic interpretation showing two Silurian-Devonian orogens between NCB, IMB, and MOB [*Tang*, 1990; *Xu et al.*, 2012]. The sedimentological constraints showing the similarity of the Upper Carboniferous to Upper Permian strata between northern NCB and southern MOB is also in agreement with our paleomagnetic data [*Mueller et al.*, 1991]. Our sedimentological study reveals that following Late Devonian molassic deposition, IMB was dominated by shallow marine carbonate platform in the Carboniferous, followed by volcanic-sedimentary sequences in the Early-Middle Permian, and continental environment with thick lacustrine sediments in the Late Permian. Consequently, no large ocean existed between NCB and MOB during the Late Paleozoic. Thus, the Paleo-Asian Ocean between NCB and MOB was closed at least since Late Devonian. NCB, IMB, and MOB were welded together as a single block. However, a small remnant sea may still exist in MOB in the Late Paleozoic, as Carboniferous arc and Permian marine sedimentary deposits were identified in south Mongolia [*Johnson*, 2004; *Heumann et al.*, 2012]. Conversely, the latitudinal differences between the welded NCB-IMB-MOB block and SIB during Devonian and Permian may correspond to the occurrence of the Mongol-Okhotsk Ocean (Figure 8). As shown by the

distribution of paleomagnetic poles along small circles centered on the sampling regions, the welded NCB-IMB-MOB block is not totally rigid owing to intracontinental deformation and significant relative rotations between NCB, IMB, and MOB domains (Figures 8a and 8b). The rotations are due to transcurrent tectonics that has been already described by the previous studies [*Enkin et al*., 1992; *Kravchinsky et al*., 2002a; *Metelkin et al*., 2010] and documented by numerous Mesozoic shear zones in MOB and IMB (e.g., East Gobi Fault zone) [*Lamb et al*., 1999, 2008; *Webb et al*., 2010].

6. Conclusions

[54] Despite the difficult outcrop conditions, we collected samples over a 3 year period and now present the first paleomagnetic data from central-eastern Inner Mongolia. Magnetic mineralogical analyses show titanium-poor magnetite and hematite as the principal magnetic carriers. From sites showing magnetization of primary origin, we have calculated a Late Devonian pole and a Permian one for IMB. Two stages of remagnetization have been also identified, probably due to Early Permian and Early Cretaceous thermal events. Although the results are still preliminary and remain qualitative, the comparison of our paleomagnetic with available poles from NCB, MOB, and SIB infers that (1) the Paleo-Asian Ocean has been closed to form a single welded block (NCB-IMB-MOB) since at least Late Devonian and (2) intracontinental deformation within NCB-IMB-MOB block has continued throughout the late Paleozoic and the Mesozoic, due to strike-slip movements along unit boundaries or within units. To improve the results from this study and better understand the Paleozoic evolution of CAOB, the study area needs to be widened. Investigating the western extension and especially the connection with the western part of CAOB (e.g., Tianshan, Altay) may be a key challenge for the late Paleozoic tectonics of Asia.

Appendix A: Analyses of Magnetic Mineralogy

[55] The analyses of magnetic mineralogy of 9 localities in this study are detailed described in the following.

A.1. North Margin of NCB

A.1.1. Damaoqi Area (S3x and D1c)

[56] For the yellow sandstone of the Upper Silurian Xibiehe Formation (S_3x), the heating curve of the magnetic susceptibility displays a quick decrease from ambient temperature to about 150°C, a progressive decrease until to 450°C, an abrupt drop from 540°C to 580°C, and a final slow decrease from 580°C to 700°C (Figure A1a), indicating the coexistence of several magnetic minerals with different Curie temperatures. In addition, an important change of the magnetic mineralogy is recorded during thermomagnetic experiments, since the magnetic susceptibility significantly increases after heating up to about 700°C (inset figure of Figure A1a) due to probable oxidation of pyrite into magnetite and pyrrhotite. IRM measurements reveal that after a rapid increase up to 200 mT, the magnetic remanence increases progressively with applied magnetic field without any saturation at 1 T (Figure A2a-1), suggesting the existence of both low and high coercive magnetic minerals in the rock.

[57] For the red sandstone of the Lower Devonian Chaganhebu Formation (D_1c), the heating curve of the magnetic susceptibility successively displays a quick decrease from ambient temperature to about 150°C, a slow decrease until 450°C, an abrupt rise from 450°C to 540°C, and an abrupt drop from 540°C to 700°C (Figure A1b), indicating the presence of several magnetic minerals with different Curie temperatures. Curie temperature measurements also reveal important change of magnetic mineralogy during experiments, as the heating and cooling curves do not overlap and the magnetic susceptibility significantly increases with cooling (inset figure of Figure A1b). This may be due to the oxidation of pyrite into magnetite and pyrrhotite. IRM measurements display a rapid increase up to 200 mT, followed by a progressive increase of the magnetic remanence with applied magnetic field without reaching saturation at 1 T (Figure A2a-2); this indicates that both low and high coercive magnetic minerals occur in the rock.

A.1.2. Aohanqi Area (C1h)

[58] For the black limestone of the Lower Carboniferous Houfangshengou Formation (C_1h), thermomagnetic curves present a slow decrease of magnetic susceptibility followed by a rapid increase from 400°C to 500°C, a sudden and severe drop from 500°C to 580°C, and finally a slow decrease from 580°C to 700°C (Figure A1c), indicating the presence of several magnetic minerals with different Curie temperatures. The diagram deduced from IRM measurements shows an abrupt increase from 0 mT to 300 mT, reaching a 90% magnetic saturation at about 300 mT (Figure A2a-3), suggesting predominantly low coercive magnetic minerals, like magnetite in the rocks.

A.2. Inner Mongolia Block (IMB)

A.2.1. Sunidzuoqi Area (D3s)

[59] For the red coarse sandstone of the Upper Devonian Seribayanaobao Formation (D_3s), the heating curve of the Curie temperature measurements displays an obvious increase of the magnetic susceptibility at about 150°C followed by a progressive increase until to a peak at about 300°C, which may correspond to the transformation of goethite and/or pyrite into pyrrhotite and/or magnetite (Figure A1d). Then an abrupt decrease from 300°C to 400°C is potentially due to maghemite destabilization (Figure A1d). The severe drop from 560°C to 600°C indicates the occurrence of titanium-poor magnetite (Figure A2d). Besides, thermomagnetic plots show an important change of the magnetic mineralogy during experiments, as the magnetic susceptibility displays a rapid increase of magnetic susceptibility at about 150°C followed by a slow increase until to a peak at about 300°C (Figure A1d).

A.2.2. Abagaqi Area (D3s)

[60] For the yellow siltstone of the Upper Devonian Seribayanaobao Formation, thermomagnetic measurements display a progressive decrease of the magnetic susceptibility to reach a plateau at 350°C and an abrupt drop from 540°C to 580°C, with a slow decrease until 700°C (Figure A1e), revealing titanium-poor magnetite. IRM measurements show a rapid increase of the magnetic remanence with applied magnetic field from 0 mT to 100 mT, followed by secondary increase from 400 without saturation at 1 T (Figure A2b-1); this suggests that both low and high coercive magnetic minerals in the rocks.

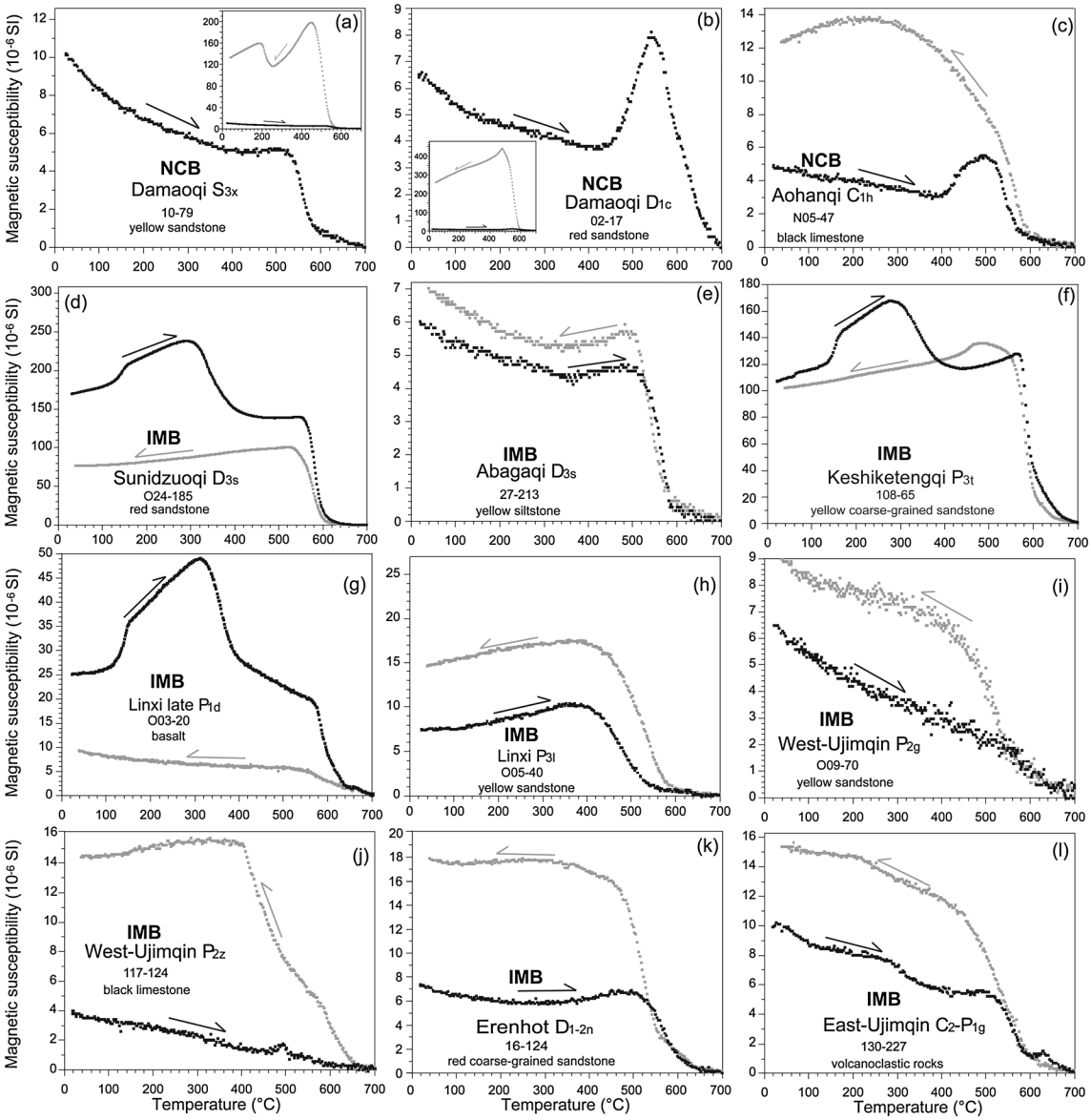


Figure A1. Representative results of thermomagnetic experiments from each sampled locality. Black (grey) curve represents heating (cooling) curve.

A.2.3. Keshiketengqi Area (P3t)

[61] For the coarse sandstone of the Upper Permian Tieyingzi Formation, thermomagnetic curves display an obvious increase of the magnetic susceptibility at about 150°C, a slow increase until to a peak at about 300°C, an abrupt decrease from 300°C to 400°C to reach a plateau, an abrupt drop from 580°C to 600°C, and a final slow decrease until 700°C (Figure A1f), indicating that both low (goethite and maghemite) and high (magnetite and hematite) Curie temperature magnetic minerals occur in the rocks. IRM measurements show an abrupt increase up to a 90% magnetic saturation from 0 mT to 300 mT, suggesting the predominance of low-coercive magnetic minerals in the rocks (Figure A2b-2).

A.2.4. Linxi Area (Late P1d and P3l)

[62] For the tuff and basalt of the upper part of the Lower Permian Dashizhai Formation (P_1d), the heating curve of the Curie temperature measurements displays a rapid increase of the magnetic susceptibility at 120–150°C, followed by a slow increase until to a peak at about 300°C, which may correspond to the transformation of goethite and/or pyrite into pyrrhotite and/or magnetite (Figure A1g). The abrupt decrease from 300°C to 400°C is potentially due to maghemite destabilization (Figure A1g). After a slow decrease between 400°C and 580°C, the susceptibility dramatically drops from 580°C to 640°C indicating the occurrence of titanium-poor magnetite and minor hematite (Figure A1g).

[63] For the sandstone of the Upper Permian Linxi Formation (P_3l), thermal magnetic measurement shows a quick decrease from 400°C to 560°C (Figure A1h), indicating titanium magnetite is probably the main remanent carrier.

A.2.5. West Ujimqin Area (C2a, P2g, and P2z)

[64] For the limestone of the Upper Carboniferous Amushan Formation (C_2a), IRM measurements show an abrupt increase up to approximately 90% saturation at about 300 mT (Figure A2b-3), indicating a predominance of low-coercivity minerals like magnetite in the rocks.

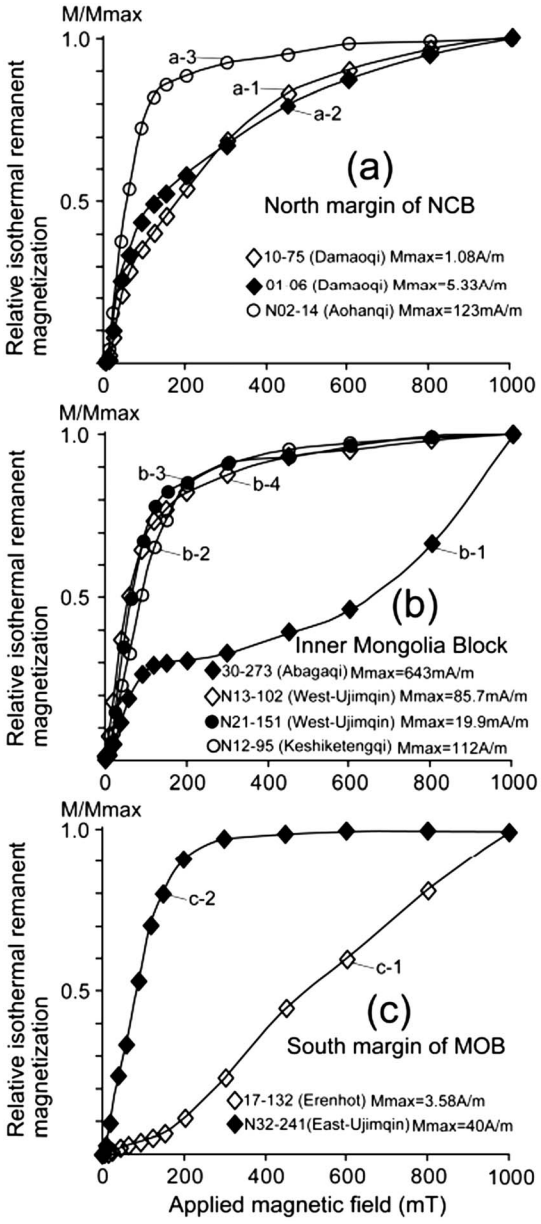


Figure A2. Representative results of isothermal magnetization measurements from each sampled locality.

[65] For the Middle Permian yellow sandstone of Gegenaobao Formation (P_2g), thermal magnetic measurements present a progressive decrease of the magnetic susceptibility from 0°C to 700°C, indicating both magnetite and hematite as the magnetic carriers (Figure A1i).

[66] For the limestone of the Middle Permian Zhesi Formation (P_2z), the heating curve of the thermomagnetic measurements presents a progressive decrease of magnetic susceptibility from 0°C to 700°C, whereas the cooling curve displays a quick increase from 700°C to 400°C (Figure A1j). Since heating and cooling curves do not overlap, changes of the magnetic mineralogy due to oxidation may occur during experiments. IRM measurements show an abrupt increase with approximately 90% saturation at about 300 mT (Figure A2b-4), indicating low-coercive magnetite may be the main magnetic carrier in the rocks.

A.3. South Margin of MOB

A.3.1. Erenhot Area (D1-2n)

[67] For the red coarse sandstone of Lower-Middle Devonian Niqiuhe Formation ($D_{1\text{-}2}n$), thermal magnetic measurements display a gradual drop from 500°C to 660°C (Figure A1h), indicating the coexistence of both magnetite and hematite as the magnetic carriers in the rock. IRM measurements show a first increase below 200 mT and a secondary sharp increase without reaching a total saturation up to 1 T (Figure A2c-1); this suggests that hematite is probably the main magnetic minerals.

A.3.2. East Ujimqin (C2-P1g)

[68] For the volcaniclastic rocks of the Upper Carboniferous-Lower Permian Gegenaobao Formation (C_2-P_1g), thermal magnetic measurements show a progressive decrease of the magnetic susceptibility with three successive drops at about 300°C, 540–580°C, and 620–680°C (Figure A1l), indicating the coexistence of maghemite, magnetite, and hematite, respectively. IRM measurements show a rapid increase to reach a total saturation at about 300 mT (Figure A2c-2), suggesting that a low-coercivity mineral like magnetite is the main magnetic carrier.

Appendix B: Anisotropy of Magnetic Susceptibility Data

Table B1. Anisotropy of Magnetic Susceptibility Data for the Sites That are Included in Mean Direction Calculations[a]

		Km	Standard Deviation			K_1				K_3			
Site	n	(10^{-6}SI)	(10^{-6}SI)	P_j	T	Dec (deg)	Inc (deg)	α_{95}max	α_{95}min	Dec (deg)	Inc (deg)	α_{95}max	α_{95}min
01	10	4.02E-04	2.29E-05	1.032	-0.216	284.9	22.2	7.7	4.3	152.4	58.9	9.2	3.6
02	11	1.41E-04	6.52E-06	1.033	0.169	253.6	25.9	7.8	4.4	111.2	58.4	6.2	2.5
03	8	3.67E-04	7.32E-05	1.053	-0.023	263.2	12.5	8.2	3	79.4	77.4	11.2	4.6
04	7	2.89E-04	7.03E-05	1.034	0.129	263.6	1.1	11.4	5.4	358.7	77.5	11.8	6.1
05	7	2.86E-04	6.75E-05	1.031	0.179	264.3	0.4	15.7	10.5	173	74.5	14	10.6
06	7	2.84E-04	5.99E-05	1.039	-0.114	268.6	18.8	6.5	5	116.8	68.9	7.8	6.1
07	8	3.48E-04	6.64E-05	1.04	0.247	259.2	5	19	1.5	114.9	83.8	10.7	2.9
08	8	3.09E-04	4.86E-05	1.045	0.582	310.2	19.7	55.2	15.2	110.7	69.2	31.9	10
09	9	1.01E-04	9.03E-05	1.015	-0.091	66.7	4.2	29.8	12.5	160.7	44	17.5	13
10	11	1.70E-04	1.07E-04	1.009	0.239	54	2.9	16.6	7.7	177.8	84.8	18.9	13.1
12	10	2.83E-04	4.26E-05	1.013	-0.123	255.5	10.7	11.2	5.8	129.2	72.3	18	6.8

Table B1. (continued)

		Km	Standard Deviation			K_1				K_3			
Site	n	(10^{-6}SI)	(10^{-6}SI)	P_j	T	Dec (deg)	Inc (deg)	α_{95}max	α_{95}min	Dec (deg)	Inc (deg)	α_{95}max	α_{95}min
13	9	3.63E-04	1.71E-05	1.024	0.235	97.9	16	32.7	3.1	207.5	49.4	13.5	7.5
14	9	1.57E-04	3.90E-05	1.014	0.462	50.5	14	22	4.3	172.5	64.8	13.7	3.8
15	9	3.30E-04	2.37E-05	1.02	0.235	234.1	0.6	35.9	13.1	328	81.1	29.2	18.7
16	8	1.55E-04	2.22E-05	1.012	0.36	139.6	27.4	44.1	9.8	252.9	37.3	28.4	9.7
17	9	2.89E-04	1.54E-04	1.01	0.366	113.2	18.7	18.7	6.2	270.9	70	9.9	6.5
18	8	1.53E-04	4.65E-05	1.048	0.413	110	14.9	33	8.7	18.9	4.3	58.4	8.1
19	9	3.92E-04	8.46E-05	1.008	0.176	317.5	24.2	21.4	17.4	96.6	59.3	23.9	20.3
20	9	3.88E-04	8.35E-05	1.006	0.322	35.7	17.2	27.6	8	203.8	72.4	24	8
21	9	1.56E-04	4.65E-05	1.006	0.308	223.5	81.7	66.4	14.9	53.6	8.2	51	20
22	8	2.17E-04	4.37E-05	1.003	-0.154	259.3	57.7	43	24.2	31.6	22.9	68.4	20.5
23	10	3.39E-04	1.12E-04	1.007	0.289	249.5	4.8	73.7	10.3	148.7	65.7	12.5	7.6
24	7	2.34E-04	3.00E-05	1.005	-0.099	330.2	4.7	13.6	8.7	61.4	14.5	32.1	6.4
N01	8	4.03E-05	1.37E-05	1.021	-0.414	127.8	73.7	21.1	9.2	15.1	6.4	70.7	11.3
N02	11	2.28E-05	8.40E-06	1.032	-0.004	46.4	1.6	13	10.3	315.4	30.7	27.8	12.6
N03	12	1.42E-05	6.93E-06	1.049	0.038	47.9	18	54.4	15.9	302.3	39.7	23.6	17.3
N04	8	3.41E-05	1.62E-05	1.018	0.236	69	31.6	83.2	28.8	291	50.4	38.2	32.2
N05	9	9.45E-06	4.37E-06	1.088	0.335	27.6	1.4	57.2	12.7	296.8	28.9	14.2	9.9
N06	8	1.74E-05	6.60E-06	1.054	0.474	241.2	35.4	82.9	9.3	143.7	10.4	13.7	3.7
N07	8	2.83E-05	5.96E-06	1.032	0.44	247.2	66.3	41.7	7.2	134.9	9.4	8.5	7.1
N08	6	1.20E-02	3.76E-03	1.022	0.275	45.4	13.5	29.9	9	300	48	45.6	12.7
N09	7	1.78E-02	3.94E-03	1.041	0.174	46.5	15.1	8	2.7	203.1	73.6	11.2	5.3
N10	6	7.58E-03	2.37E-03	1.027	-0.233	201.8	17.5	13	3.5	56.9	69	27.1	4.9
N11	7	4.72E-03	2.81E-03	1.022	-0.084	210.2	33.8	9.2	3.6	112.3	11.5	55.6	5
N12	6	6.03E-03	1.14E-03	1.027	-0.414	199.1	22.8	6.2	3.2	74.5	53.5	17.3	3
N13	7	2.15E-05	4.20E-06	1.036	-0.274	203.4	31.6	14.3	8.8	337.4	48.5	32.3	12.9
N14	6	2.76E-05	9.12E-06	1.073	0.165	270.1	10.5	42.6	5.3	172.2	36.6	33.9	3.7
N15	6	3.13E-05	8.28E-06	1.075	-0.256	103.2	5.1	5.7	3.3	206.8	69.2	27	2.9
N16	6	2.25E-05	1.35E-06	1.031	-0.135	99.8	17.2	45.5	3.2	202	34.4	13.1	4.2
N17	6	3.65E-05	8.61E-06	1.051	-0.117	100	4.1	23.5	2.9	195.1	51.1	49.5	3
N18	5	3.21E-05	7.54E-06	1.045	0.026	104.3	3.2	31.7	3	200	60.8	32.7	2.8
N27	7	3.76E-03	3.81E-03	1.126	-0.282	220	11.9	8.5	3.3	24.3	77.7	31.6	8.4
N28	7	2.07E-03	2.88E-03	1.057	-0.446	221.1	11.9	3.9	2.9	316.7	24.9	23	2.1
N29	8	2.25E-04	9.17E-05	1.017	-0.258	171.7	23	10.8	2.7	316	62.5	26.4	2.7
N30	9	2.52E-03	5.81E-03	1.036	-0.408	176.4	10.3	43.8	6.7	323.9	77.9	27.5	7.4
N31	8	9.44E-03	4.62E-03	1.1	-0.409	215.1	9.6	4.3	3.3	10.9	79.5	17.1	3.3
N32	10	2.40E-03	2.00E-03	1.115	-0.325	219.8	9	4	2.2	311.2	8.7	15.2	2.6
O05-06	9	2.20E-04	2.17E-05	1.028	-0.053	283	10.9	29.9	9.1	188.2	23.4	16.8	9.6
O07-14	11	4.64E-03	9.30E-03	1.058	0.514	30	22.4	13.8	12.2	120.3	0.6	23.4	4.9
O16-17	9	1.88E-03	6.55E-04	1.033	0.256	182.7	0.2	21	4.6	91.6	80.2	4.9	2.7
O23-25	9	3.41E-03	2.14E-03	1.036	0.346	359	11.9	10.6	4.7	210.7	76.1	6.2	4.5

[a]Site numbers are the same as that of Table 1. Samples from Upper Devonian in Abagaqi (sites 25–30) and Upper Carboniferous in West Ujimqin (sites N19–N26) are excluded as no mean directions or PEF directions are calculated. $P_J = \exp\{2[(\ln K_1 - \ln K_m)^2+(\ln K_2 - \ln K_m)^2+(\ln K_3 - \ln K_m)^2]^{1/2}\}$, and $T = 2\ln(K_2/K_3)/\ln(K_1/K_3) - 1)$. K_1 and K_3 are principal axes of the magnetic fabrics. K_1: magnetic lineation; K_3: pole of the magnetic foliation; Dec/Inc: declination/inclination. α_{95}max/α_{95}min: the maximum/minimum radius that mean direction lies within 95% confidence.

[69] **Acknowledgments.** We thank Wei Wei for the technical help in the laboratory and AMS analyses. We thank Tong Qinlong, Li Ruibiao, Fang Junqin, and Cheng Shengdong for their support in the field. We gratefully acknowledge the Associate Editor Stuart Gilder, Cari Johnson, and another anonymous reviewer for their constructive comments that considerably improved this manuscript. This study was supported by grants from the National Natural Science Foundation of China (40872145, 40821002). This is a contribution to IGCP 592 supported by UNESCO-IUGS.

References

Blight, J. H. S., Q. G. Crowley, M. G. Petterson, and D. Cunningham (2010), Granites of the Southern Mongolia Carboniferous Arc: New geochronological and geochemical constraints, *Lithos*, *116*, 35–52, doi:10.1016/j.lithos.2010.01.001.

Charles, N., Y. Chen, R. Augier, C. Gumiaux, W. Lin, M. Faure, P. Monié, F. Choulet, F. Y. Wu, R. X. Zhu, and Q. C. Wang (2011), Palaeomagnetic constraints from granodioritic plutons (Jiaodong Peninsula): New insights on Late Mesozoic continental extension in Eastern Asia, *Phys. Earth. Planet. In.*, *187*, 276–291, doi:10.1016/j.pepi.2011.05.006.

Chen, B., B. M. Jahn, S. Wilde, and B. Xu (2000), Two contrasting Paleozoic magmatic belts in northern Inner Mongolia, China: Petrogenesis and tectonic implications, *Tectonophysics*, *328*, 157–182, doi:10.1016/S0040-1951(00)00182-7.

Chen, C., Z. C. Zhang, Z. J. Guo, J. F. Li, Z. S. Feng, and W. H. Tang (2012), Geochronology, geochemistry, and its geological significance of the Permian Mandula mafic rocks in Damaoqi, Inner Mongolia, *Sci. China Earth Sci.*, *55*, 39–52, doi:10.1007/s11430-011-4277-z.

Cogné, J. P. (2003), A Macintosh^{TM} application for treating paleomagnetic data and making plate reconstructions, *Geochem. Geophys. Geosyst.*, *4*(1), 1007, doi:10.1029/2001GC000227.

Cogné, J. P., V. A. Kravchinsky, N. Halim, and F. Hankard (2005), Late Jurassic–Early Cretaceous closure of the Mongol-Okhotsk Ocean demonstrated by new Mesozoic palaeomagnetic results from the Trans-Baikal area (SE Siberia), *Geophys. J. Int.*, *163*, 813–832, doi:10.1111/j.1365-246X.2005.02782.X.

Cottrell, R. D., J. A. Tarduno, and J. Roberts (2008), The Kiaman Reversed Polarity Superchron at Kiama: Toward a field strength estimate based on single silicate crystals, *Phys. Earth. Planet. Inter.*, *169*, 49–58, doi:10.1016/j.pepi.2008.07.041.

Daoudene, Y., D. Gapais, G. Ruffet, E. Gloaguen, A. Cocherie, and P. Ledru (2012), Syn-thinning pluton emplacement during Mesozoic extension in eastern Mongolia, *Tectonics*, *31*, TC3001, doi:10.1029/2011TC002926

De Jong, K., W. J. Xiao, B. F. Windley, H. Masago, and C. H. Lo (2006), Ordovician $^{40}Ar/^{39}Ar$ phengite ages from the blueschist-facies Ondor

Sum subduction-accretion complex (Inner Mongolia) and implications for the early Paleozoic history of continental blocks in China and adjacent areas, *Am. J. Sci.*, *306*, 799–845, doi:10.2475/10.2006.02.

Demoux, A., A. Kroner, D. Y. Liu, and G. Badarch (2007), Precambrian crystalline basement in southern Mongolia as revealed by SHRIMP zircon dating, *Int. J. Earth Sci.*, *98*, 1365–1380, doi:10.1007/s00531-008-0321-4.

Enkin, R. J. (2003), The direction-correction tilt test: An all-purpose tilt/fold test for paleomagnetic studies, *Earth Planet. Sci. Lett.*, *212*, 151–166, doi:10.1016/S0012-821X(03)00238-3.

Enkin, R. J., Z. Y. Yang, Y. Chen, and V. Courtillot (1992), Paleomagnetic constraints on the geodynamic history of the major blocks of China from the Permian to the present, *J. Geophys. Res.*, *97*, 13953–13989, doi:10.1029/92JB00648.

Fisher, R. (1953), Dispersion on a sphere, *Proc. R. Soc. London, Ser. A*, *217*, 295–305.

Garcia, A. S., D. N. Thomas, D. Liss, and J. Shaw (2006), Low geomagnetic field intensity during the Kiaman superchron: Thellier and microwave results from the Great Whin Sill intrusive complex, northern United Kingdom, *Geophys. Res. Lett.*, *33*, L16308, doi:10.1029/2006GL026729

Ge, M., W. Zhou, Y. Yu, J. Sun, J. Bao, and S. Wang (2011), Dissolution and supracrustal rocks dating of Xilin Gol Complex, Inner Mongolia, China (in Chinese with English abstract), *Earth Sci. Frontiers*, 2011, *18*(5), 182–195.

Graham, S. A., M. S. Hendrix, C. L. Johnson, D. Badamgarav, G. Badarch, J. Amory, M. Porter, R. Barsbold, L. E. Webb, and B. R. Hacker (2001), Sedimentary record and tectonic implications of Mesozoic rifting in southeast Mongolia, *Geol. Soc. Am. Bull.*, *113*, 1560–1579, doi:10.1130/0016-7606(2001)113<1580:PTMATC>2.0.CO;2.

Halim, N., V. Kravchinsky, S. Gilder, J. P. Cogne, M. Alexyutin, A. Sorokin, V. Courtillot, and Y. Chen (1998), A palaeomagnetic study from the Mongol–Okhotsk region: Rotated Early Cretaceous volcanics and remagnetized Mesozoic sediments, *Earth Planet. Sci. Lett.*, *159*, 133–145, doi:10.1016/S0012-821X(98)00072-7.

Han, J., J. B. Zhou, X. Z. Zhang, and H. J. Qiu (2011), Detrital zircon U-Pb dating from sandstone of the Upper Permian Linxi Formation, Linxi area, Inner Mongolia, China and its tectonic implications (in Chinese with English abstract), *Geol. Bull. China*, *30*, 258–269.

Heumann, M. J., C. L. Johnson, L. E. Webb, J. P. Taylor, U. Jalbaa, and C. Minjin (2012), Paleogeographic reconstruction of a late Paleozoic arc collision zone, southern Mongolia, *Geol. Soc. Am. Bull.*, *124*, 1514–1534, doi:10.1130/B30510.1.

Huang, B. C., Y. Otofuji, Z. Y. Yang, and R. X. Zhu (2000), New Silurian and Devonian palaeomagnetic results from the Hexi Corridor terrane, northwest China, and their tectonic implications, *Geophys. J. Int.*, *140*, 132–146, doi:10.1046/j.1365-246x.2000.00983.x.

Huang, B. C., Y. Otofuji, R. X. Zhu, R. P. Shi, and Y. C. Wang (2001), Paleomagnetism of Carboniferous sediments in the Hexi Corridor: Its origin and tectonic implications, *Earth Planet. Sci. Lett.*, *194*, 135–149, doi:10.1016/S0012-821X(01)00557-X.

IMBGMR (Inner Mongolian Bureau of Geology and Mineral Resources) (1991), *Regional Geology of Inner Mongolian Autonomous Region (in Chinese with English abstract)*, pp. 1–725, Geological Publishing House, Beijing.

IMBGMR (Inner Mongolian Bureau of Geology and Mineral Resources) (2002), Regional Geological Investigation Report of 1:250000 scale BaiyunObo Quadrangle (in Chinese), Inner Mongolian Bureau of Geology and Mineral Resources.

Jahn, B. M., B. A. Litvinovsky, A. N. Zanvilevich, and M. Reichow (2009), Peralkaline granitoid magmatism in the Mongolian–Transbaikalian Belt: Evolution, petrogenesis and tectonic significance, *Lithos*, *113*, 521–539, doi:10.1016/j.lithos.2009.06.015.

Jelínek, V. (1978), Statistical processing of anisotropy of magnetic susceptibility measured on groups of specimen, *Stud. Geofyz. Geodet.*, *22*, 50–62.

Jian, P. et al. (2008), Time scale of an early to mid-Paleozoic orogenic cycle of the long-lived Central Asian Orogenic Belt, Inner Mongolia of China: Implications for continental growth, *Lithos*, *101*, 233–259, doi:10.1016/j.lithos.2007.07.005.

Jian, P., A. Kröner, B. F. Windley, Y. Shi, W. Zhang, L. Zhang, and W. Yang (2012), Carboniferous and Cretaceous mafic-ultramafic massifs in Inner Mongolia (China): A SHRIMP zircon and geochemical study of the previously presumed integral "Hegenshan ophiolite", *Lithos*, *142-143*, 48–66, doi:10.1016/j.lithos.2012.03.007.

Johnson, C. L. (2004), Polyphase evolution of the East Gobi basin: Sedimentary and structural records of Mesozoic-Cenozoic intraplate deformation in Mongolia, *Basin Res.*, *16*, 79–99, doi:10.1046/j.1365-2117.2003.00221.X.

Johnson, C. L., J. A. Amory, D. Zinniker, M. A. Lamb, S. A. Graham, M. Affolter, and G. Badarch (2008), Sedimentary response to arc-continent collision, Permian, southern Mongolia, in *Formation and Applications of the Sedimentary Record in Arc Collision Zones*, edited by A. E. Draut, P. D. Clift, and D. W. Scholl, Geol. Soc. Am. Spec. Paper, *436*, pp. 363–390, Geological Society of America, Boulder, Colo.

Kirschvink, J. L. (1980), The least-squares line and plane and the analysis of paleomagnetic data, *Geophys. J. R. Astron. Soc.*, *62*, 699–718, doi:10.1111/j.1365-246X.1980.tb02601.X.

Kravchinsky, V. A., A. A. Sorokin, and V. Courtillot (2002a), Paleomagnetism of Paleozoic and Mesozoic sediments from the southern margin of Mongol-Okhotsk ocean, far eastern Russia, *J. Geophys. Res.*, *107*(B10), 2253, 2253, doi:10.1029/2001JB000672

Kravchinsky, V. A., J. P. Cogné, W. Harbert, and M. I. Kuzmin (2002b), Evolution of the Mongol-Okhotsk Ocean with paleomagnetic data from the suture zone, *Geophys. J. Int.*, *148*, 34–57, doi:10.1046/j.1365-246x.2002.01557.X.

Kravchinsky, V. A., K. M. Konstantinov, V. Courtillot, J. I. Savrasov, J. P. Valet, S. D. Cherniy, S. G. Mishenin, and B. S. Parasotka (2002c), Palaeomagnetism of East Siberian traps and kimberlites: Two new poles and palaeogeographic reconstructions at about 360 and 250 Ma, *Geophys. J. Int.*, *148*, 1–33, doi:10.1046/j.0956-540x.2001.01548.X.

Kröner, A., J. Lehmann, K. Schulmann, A. Demoux, O. Lexa, D. Tomurhuu, P. Štípská, D. Liu, and M. T. D. Wingate (2010), Lithostratigraphic and geochronological constraints on the evolution of the Central Asian Orogenic Belt in SW Mongolia: Early Paleozoic rifting followed by late Paleozoic accretion, *Am. J. Sci.*, *310*, 523–574, doi:10.2475/07.2010.01.

Lamb, M. A., A. D. Hanson, S. A. Graham, G. Badarch, and L. E. Webb (1999), Left-lateral sense offset of upper Proterozoic to Paleozoic features across the Gobi Onon, Tost, and Zuunbayan faults in southern Mongolia and implications for other Central Asian faults, *Earth Planet. Sci. Lett.*, *173*, 183–194, doi:10.1016/S0012-821X(99)00227-7.

Lamb, M. A., G. Badarch, T. Navratil, and R. Poier (2008), Structural and geochronologic data from the Shin Jinst area, eastern Gobi Altai, Mongolia: Implications for Phanerozoic intracontinental deformation in Asia, *Tectonophysics*, *451*, 312–330, doi:10.1016/j.tecto.2007.11.061.

Lehmann, J., K. Schulmann, O. Lexa, M. Corsini, A. Kröner, P. Štípská, D. Tomurhuu, and D. Otgonbator (2010), Structural constraints on the evolution of the central Asian Orogenic Belt In SW Mongolia, *Am. J. Sci.*, *310*, 575–628, doi:10.2475/07.2010.02.

Li, J. Y. (2006), Permian geodynamic setting of Northeast China and adjacent regions: Closure of the Paleo-Asian Ocean and subduction of the Paleo-Pacific Plate, *J. Asian Earth Sci.*, *26*, 207–224, doi:10.1016/j.jseaes.2005.09.001.

Litvinovsky, B. A., A. A. Tsygankov, B. M. Jahn, Y. Katzir, and Y. Be'eri-Shlevin (2011), Origin and evolution of overlapping calc-alkaline and alkaline magmas: The late Palaeozoic post-collisional igneous province of Transbaikalia (Russia), *Lithos*, *125*, 845–874, doi:10.1016/j.lithos.2011.04.007.

Liu, J. F. (2009), Late Paleozoic magmatism and its constraints on regional tectonic evolution in Linxi-Dongwuqi area, Inner Mongolia (in Chinese with English abstract), Doc. thesis, Univ. of Jilin, Changchun, Jilin, China

Liu, W., W. Siebel, X. J. Li, and X. F. Pan (2005), Petrogenesis of the Linxi granitoids, northern Inner Mongolia of China: Constraints on basaltic underplating, *Chem. Geol.*, *219*, 5–35, doi:10.1016/j.chemgeo.2005.01.013.

Luo, H. L., T. R. Wu, and L. Zhao (2009), Zircon SHRIMP U-Pb dating of Wuliangsitai A-type granite on the northern margin of the North China Plate and tectonic significance (in Chinese with English abstract), *Acta Petrol. Sin.*, *25*(3), 515–526.

McElhinny, M. W., B. J. J. Embleton, X. H. Ma, and Z. K. Zhang (1981), Fragmentation of Asia in the Permian, *Nature*, *293*, 212–216.

McFadden, P. L., and M. W. McElhinny (1988), The combined analysis of remagnetization circles and direct observations in paleomagnetism, *Earth Plant. Sci. Lett.*, *87*, 161–172, doi:10.1016/0012-821X(88)90072-6.

McFadden, P. L., and M. W. McElhinny (1990), Classification of the reversal test in palaeomagnetism, *Geophys. J. Int.*, *103*, 725–729, doi:10.1111/j.1365-246X.1990.tb05683.X.

Meng, Q. R. (2003), What drove late Mesozoic extension of the northern China-Mongolia tract?, *Tectonophysics*, *369*, 155–174, doi:10.1016/S0040-1951(03)00195-1.

Meng, Z., H. F. Huang, Y. Z. Chen, and R. S. Coe (1990), The Late Permian pole of the western Jiuquan Basin (NW China) and its tectonic implication, *Acta Sedment. Sin.*, *8*, 58–65.

Metelkin, D. V., V. A. Vernikovsky, A. Y. Kazansky, and M. T. D. Wingate (2010), Late Mesozoic tectonics of Central Asia based on paleomagnetic evidence, *Gond. Res.*, *18*, 400–419, doi:10.1016/j.gr.2009.12.008.

Miao, L., F. Zhang, W. M. Fan, and D. Liu (2007), Phanerozoic evolution of the Inner Mongolia-Daxinganling orogenic belt in North China: Constraints from geochronology of ophiolites and associated formations, *Geol. Soc. London, Spec. Pub.*, *280*, 223–237, doi:10.1144/SP280.11.

Miao, L., W. Fan, D. Liu, F. Zhang, Y. Shi, and F. Guo (2008), Geochronology and geochemistry of the Hegenshan ophiolitic complex: Implications

for late-stage tectonic evolution of the Inner Mongolia-Daxinganling Orogenic Belt, China, *J. Asian Earth Sci.*, *32*, 348–370, doi:10.1016/j.jseaes.2007.11.005.

Mueller, J. F., J. J. W. Rogers, Y. G. Jin, H. Wang, W. Li, J. Chronic, and J. F. Mueller (1991), Late Carboniferous to Permian sedimentation in Inner Mongolia, China, and tectonic relationships between north China and Siberia, *J. Geol.*, *99*, 251–263.

Pavlov, V. E., V. Courtillot, M. L. Bazhenov, and R. V. Veselovsky (2007), Paleomagnetism of the Siberian traps: New data and a new overall 250 Ma pole for Siberia, *Tectonophysics*, *443*, 72–92, doi:10.1016/j.tecto.2007.07.005.

Pisarevsky, S. A., D. P. Gladkochub, T. A. Donskaya, B. De Waele, and A. M. Mazukabzov (2006), Palaeomagnetism and geochronology of mafic dykes in south Siberia, Russia: The first precisely dated Early Permian palaeomagnetic pole from the Siberian craton, *Geophys. J. Int.*, doi:10.1111/j.1365-246X.2006.03160.X.

Pruner, P. (1987), Palaeomagnetism and palaeogeography of Mongolia in the Cretaceous, Permian and Carboniferous-preliminary data, *Tectonophysics*, *139*, 155–167, doi:10.1016/0040-1951(87)90204-6.

Pruner, P. (1992), Palaeomagnetism and palaeogeography of Mongolia from the Carboniferous to the Cretaceous-final report, *Phys. Earth Planet. Inter.*, *70*, 169–177, doi:10.1016/0031-9201(92)90179-Y.

Ren, J., K. Tamaki, S. Li, and J. Zhang (2002), Late Mesozoic and Cenozoic rifting and its dynamic setting in eastern China and adjacent areas, *Tectonophysics*, *344*, 175–205, doi:10.1016/S0040-1951(01)00271-2.

Sengör, A. M. C., B. A. Natal'in, and V. S. Burtman (1993), Evolution of the Altaid tectonic collage and Palaeozoic crustal growth in Eurasia, *Nature*, *364*, 299–307.

Tang, K. D. (1990), Tectonic development of Paleozoic fold belts at the north margin of the Sino–Korean craton, *Tectonics*, *9*, 249–260, doi:10.1029/TC009i002p00231.

Veselovsky, R. V., Y. Gallet, and V. E. Pavlov (2003), Paleomagnetism of traps in the Podkamennaya Tunguska and Kotui River Valleys: Implications for the post-Paleozoic relative movements of the Siberian and East European platforms, *Phys. Solid Earth*, *39*, 856–871.

Wang, T., Y. Zheng, G. H. Gehrels, and Z. Mu (2001), Geochronological evidence for the existence of South Mongolian microcontinent—A zircon U-Pb age of granitoid gneisses from the Yagan-Onch Hayrhan metamorphic core complex, *Chi. Sci. Bull.*, *46*, 2005–2008, doi:10.1007/BF02901917.

Wang, C. Y., P. Wang, and W. G. Li (2004a), Gonodonts from the Permian Jisu Honguer (Zhesi) Formation of Inner Mongolia, *Geobios*, *37*, 471–480, doi:10.1016/j.geobios.2003.06.003.

Wang, T., Y. Zheng, T. Li, and Y. Gao (2004b), Mesozoic granitic magmatism in extensional tectonics near the Mongolian border in China and its implications for crustal growth, *J. Asian Earth Sci.*, *23*, 715–729, doi:10.1016/S1367-9120(03)00133-0.

Webb, L. E., and C. L. Johnson (2006), Tertiary strike-slip faulting in southeastern Mongolia and implications for Asian tectonics, *Earth Planet. Sci. Lett.*, *241*, 323–335, doi:10.1016/j.epsl.2005.10.033.

Webb, L. E., S. A. Graham, C. L. Johnson, G. Badarch, and M. S. Hendrix (1999), Occurrence, age, and implications of the Yagan–Onch Hayrhan metamorphic core complex, southern Mongolia, *Geology*, *27*, 143–146, doi:10.1130/0091-7613(1999)027<0147:RSPAIT>2.3.CO;2.

Webb, L. E., C. L. Johnson, and C. Minjin (2010), Late Triassic sinistral shear in the East Gobi Fault Zone, Mongolia, *Tectonophysics*, *495*, 246–255, doi:10.1016/j.tecto.2010.09.033.

Wei, H. H., Q. R. Meng, G. L. Wu, and L. Li (2012), Multiple controls on rift basin sedimentation in volcanic settings: Insights from the anatomy of a small Early Cretaceous basin in the Yanshan belt, northern North China, *Geol. Soc. Am. Bull.*, *124*, 380–399, doi:10.1130/B30495.1.

Windley, B. F., D. Alexeiev, W. J. Xiao, A. Kröner, and G. Badarch (2007), Tectonic models for accretion of the Central Asian Orogenic Belt, *J. Geol. Soc. London*, *164*, 31–47, doi:10.1144/0016-764920006-022.

Wu, H. N., L. F. Zhou, and Z. Y. Zhao (1993), Paleomagnetic study of Carboniferous and Permian rocks from the Alashan and surrounding regions and its tectonic implications (in Chinese), *Sci. China Ser. B*, *23*, 527–536.

Wu, F. Y., J. Q. Lin, S. A. Wilde, D. Y. Sun, and J. H. Yang (2005), Nature and significance of the Early Cretaceous giant igneous event in eastern China, *Earth Planet. Sci. Lett.*, *233*, 103–119, doi:10.1016/j.epsl.2005.02.019.

Wu, F. Y., D. Y. Sun, W. C. Ge, Y. B. Zhang, M. L. Grant, S. A. Wilde, and B. M. Jahn (2011), Geochronology of the Phanerozoic granitoids in northeastern China, *J. Asian Earth Sci.*, *41*, 1–30, doi:10.1016/j.jseaes.2010.11.014.

Xiao, W. J., B. Windley, J. Hao, and M. G. Zhai (2003), Accretion leading to collision and the Permian Solonker suture, Inner Mongolia, China: Termination of the Central Asian Orogenic Belt, *Tectonics*, *22*(6), 1069, doi:10.1029/2002TC001484

Xu, B., and B. Chen (1997), Framework and evolution of the middle Paleozoic orogenic belt between Siberian and North China Plates in northern Inner Mongolia, *Sci. China Ser. D*, *40*(5), 463–469, doi:10.1007/BF02877610.

Xu, X., W. Harbert, S. Dril, and V. Kravchinksy (1997), New paleomagnetic data from the Mongol–Okhotsk collision zone, Chita region, south-central Russia: Implications for Paleozoic paleogeography of the Mongol–Okhotsk Ocean, *Tectonophysics*, *269*, 113–129, doi:10.1016/S0040-1951(96)00140-0.

Xu, B., J. Charvet, and F. Q. Zhang (2001), Primary study on petrology and geochronology of the blueschist in Sonid Zuoqi, northern Inner Mongolia (in Chinese with English abstract), *Chin. J. Geol.*, *36*, 424–434.

Xu, B., J. Charvet, Y. Chen, P. Zhao, and G. Z. Shi (2012), Middle Paleozoic convergent orogenic belts in western Inner Mongolia (China): Framework, kinematics, geochronology and implications for tectonic evolution of the Central Asian Orogenic Belt, *Gond. Res.*, doi:10.1016/j.gr.2012.05.015.

Yang, Z. Y., X. H. Ma, B. C. Huang, Z. M. Sun, and Y. X. Zhou (1998), Apparent polar wander path and tectonic movement of the North China Block in Phanerozoic, *Sci. China Ser. D*, *41* Supp., 51–65, doi:10.1007/BF02984513.

Zhang, X. H., H. F. Zhang, Y. J. Tang, S. A. Wilde, and Z. C. Hu (2008), Geochemistry of Permian bimodal volcanic rocks from Central Inner Mongolia, North China: Implication for tectonic setting and Phanerozoic continental growth in Central Asian Orogenic Belt, *Chem. Geol.*, *249*, 261–281, doi:10.1016/j.chemgeo.2008.01.005.

Zhang, Y. P., Y. Z. Su, and J. C. Li (2010), Regional tectonics significance of the Late Silurian Xibiehe Formation in central Inner Mongolia, China, *Geol. Bull. China*, *29*(11), 1599–1605.

Zhang, X. H., S. A. Wilde, H. F. Zhang, and M. G. Zhai (2011), Early Permian high-K calc-alkaline volcanic rocks from NW Inner Mongolia, North China: Geochemistry, origin and tectonic implications, *J. Geol. Soc. London*, *168*, 525–543, doi:10.1144/0016-76492010-094.

Zhao, X. X., and R. Coe (1989), Tectonic implications of Permo-Triassic paleomagnetic results from North and South China. In: J.W. Hillhouse (Editor), Deep Structure and Past Kinematics of Accreted Terranes, *IUG-G Geophys. Monogr.*, *5*, 267–283.

Zhao, X., R. S. Coe, Y. Zhou, H. Wu, and J. Wang (1990), New paleomagnetic results from northern China: Collision and suturing with Siberia and Kazakhstan, *Tectonophysics*, *181*, 43–81, doi:10.1016/0040-1951(90)90008-V.

Zhao, X. X., R. S. Coe, H. N. Wu, and Z. Y. Zhao (1993), Silurian and Devonian palaeomagnetic poles from North China and implications for Gondwana, *Earth Planet. Sci. Lett.*, *117*, 497–506, doi:10.1016/0012-821X(93)90099-U.

Zhao, L., T. R. Wu, and H. L. Luo (2011), SHRIMP U-Pb dating, geochemistry and tectonic implications of the Beiqigetao gabbros in Urad Zhongqi area, Inner Mongolia (in Chinese with English abstract), *Acta Petrol. Sin.*, *27*(10), 3071–3082.

Zhu, R., Z. Yang, H. Wu, X. Ma, B. Huang, Z. Meng, and D. Fang (1998), Paleomagnetic constraints on the tectonic history of the major blocks of China during the Phanerozoic, *Sci. China Ser. D*, *41*, 1–19, doi:10.1007/BF02984508.

Zonenshain, L. P., M. I. Kuzmin, and L. M. Natapov (1990), *Tectonics of Lithosphere Plates of the Territory of the USSR (in Russian)*, Nedra, Moscow, vol. *1*, pp. 328.